

Sensitive dependence of trajectories on tracer seeding positions - coherent structures in German Bight ~~surface~~ backward drift simulations

Ulrich Callies¹

¹Institute of Coastal Research, Helmholtz-Zentrum Geesthacht, Max-Planck-Str. 1, 21502 Geesthacht, Germany

Correspondence: Ulrich Callies (ulrich.callies@hzg.de)

Abstract. Backward drift simulations can aid the interpretation of in situ monitoring data. ~~Some trajectories~~In some cases, however, ~~are trajectories are very~~ sensitive to even small changes of the tracer release position. A corresponding spread of backward simulations implies ~~convergence~~attraction in the forward passage of time ~~-. Such and hence~~ uncertainty about the probed water body's origin ~~complicates the interpretation of measurements~~. This study examines surface drift simulations in the German Bight (North Sea). Lines across which drift behaviour changes non-smoothly are obtained as ridges in the fields of the finite-time Lyapunov exponent (FTLE), a parameter used in dynamical systems theory to identify Lagrangian coherent structures (LCS). Results ~~are shown to~~ closely resemble those obtained considering ~~a) two-particle relative dispersion and b) the average divergence of Eulerian velocities that tracers experience. Structures observed in simulated sea surface temperature and salinity further corroborate the FTLE results. It is argued that simulated FTLE fields might be used in support of the interpretation of monitoring data, indicating also vagueness of drift simulations being used.~~

Copyright statement. Author 2020. This work is distributed under the Creative Commons Attribution 3.0 License.

1 Introduction

In the German Bight area ~~exists~~(North Sea) a comprehensive monitoring network is operated, including the Marine Environmental Monitoring Network in the North Sea (MARNET), the Coastal Observing System for the North and Arctic Seas (COSYNA) and other stations. Details on the type of data being collected can be found in Baschek et al. (2017). Stanev et al. (2016) discuss issues related to modelling and data assimilation with spatiotemporal optimal interpolation. Multivariate statistical methods ~~could~~can also be used for optimizing the design of observational arrays (e.g. Chen et al., 2016; Kim and Hwang, 2020). ~~However, data analysis based on~~When it comes to the analysis of specific data, however, a merely statistical description of spatial connectivity falls short of what can be achieved if hydrodynamic current fields from either models or remote sensing are available. ~~This applies all the more, when it comes to the interpretation of data from a whole array of in situ monitoring stations.~~

Backward ~~trajectories of Lagrangian tracers~~ tracer trajectories seeded at monitoring stations provide ~~valuable~~ insight into the background of water bodies that ~~are probed (e.g. d'Ovidio et al., 2015). They help were probed (e.g. d'Ovidio et al., 2015; Lucas et al., 2011), helping~~ distinguish between temporal and spatial variability, i.e. local changes and advection from somewhere else. ~~Because of considerable uncertainties, however, following just single particle trajectories is likely to be misleading. Trajectories accumulate deficiencies of the underlying hydrodynamic fields, including the effects of unresolved sub-grid scale hydrodynamic structures. Initially moderate deviations may possibly transfer a trajectory to another submesoscale circulation structure.~~ Backtracking water bodies from hypothetical monitoring stations in the vicinity of Helgoland, Callies et al. (2011, their Fig. 3) provide an example of how quasi-chaotic mixing ~~may transform~~ in two-dimensional barotropic simulations transforms initially regular into quite contorted structures. Also in nature, forward trajectories of drifters released pairwise may separate quite fast (e.g. Callies et al., 2019; Meyerjürgens et al., 2020), ~~which sets a limit to the reliability of simulations that can be achieved in the best case.~~ Therefore, a key question is how reliable backward drift analyses can be and how the numerical analysis of a water body's recent history should be designed. In addition to well known random dispersion there exist also flow patterns that affect separation of simulated backward trajectories more systematically (Haller, 2015). The present study focuses on this latter aspect, i.e. coherent structures shaping separation of simulated backward trajectories.

~~For these reasons, Lucas et al. (2016) for instance, studying the variation of bacterial community composition at station Helgoland Roads in the German Bight (North Sea), considered the behaviour of a whole bundle of backward trajectories, seeded within an extended region around the observational site. Uncertainties due to sub-grid scale eddies unresolved in the model were dealt with by a random walk component superimposed to each individual trajectory. This blanket approach implicitly deals also with the problem the present study focusses on: A possibly high sensitivity of backward trajectories (either simulated or observed) to where exactly they are seeded.~~ A statistical measure ~~for such of~~ particle spreading is relative dispersion, the mean square particle distance, as function of time. LaCasce (2008) reviews how this parameter relates to the energy spectrum of a turbulent flow. Relative dispersion is called local when particle separation is dominated by small eddies with a typical scale that compares with particle separation. By contrast, it is termed non-local if particle separation is dominated by eddies much larger than particle separation. In ~~this the latter~~ case, characterized by a steep energy spectrum, particle separation is expected to grow exponentially. ~~The Such~~ very high sensitivity to initial particle positions implies what in dynamical systems theory is called chaotic advection (Wiggins, 2005).

Dynamical systems theory aims at a description of the kinematics of turbulent mixing. The approach is based on flow maps that describe particle advection over some time interval, according to Haller (2015) "*thereby mimicking experimental flow visualization by tracers*". This technique has widely been applied for analysing the microstructure of chaotic mixing processes in two dimensions (e.g. Pierrehumbert and Yang, 1993), describing how chaotic advection may transform initially small disks of fluid into complex filamentary structures. Trying to improve the sometimes vague definitions of such structures, Haller and Yuan (2000) introduced the framework of Lagrangian coherent structures (LCS). Their method seeks to identify material lines that function as only weakly permeable barriers for water body transport, attracting or repelling neighbored trajectories. Peacock and Haller (2013) provide a nice overview of the topic.

~~In case of flows with arbitrary time dependence, identification of LCSs can still be difficult.~~ Attracting LCSs, in dynamical systems theory also called unstable because of a fast stretching of particles along them (according to Harrison and Glatzmaier (2010) an unfortunate historical definition), have been used for optimizing drifter deployments in field studies. Poje et al. (2002) proposed drifter deployment into attracting LCSs to ensure fast dispersal based on near-exponential material stretching, which
60 lets drifters explore regions of high kinetic energy. Molcard et al. (2006) used this approach for assimilating drifter velocities into an ocean general circulation model. Different from these studies, Shadden et al. (2009) focus on repelling LCSs. Seeding drifters in a less localized way, Shadden et al. try to make drifters stay as long as possible in a specific region delineated by transport barriers. They exemplify that a LCS's robustness might enable extrapolation of its separatrix function even beyond the time horizon of detailed operational hydrodynamic predictions (e.g. three days). Combining SeaWiFS ocean-colour data
65 with altimetry-derived surface currents in the Brazil-Malvinas confluence zone, d'Ovidio et al. (2010) found that stirring by mesoscale currents can play an important role in structuring phytoplankton communities and even create what they call fluid dynamical niches, sharply delimited by LCSs. Hernández-Carrasco et al. (2018) study this topic at the submesoscale, using currents observed with High-Frequency Radar (HFR) in coastal waters. According to Scales et al. (2018) attracting LCSs can also be targeted by fisheries, led by lines of drifting foam or debris.

70 Conducting backward simulations, the present study proposes the use of LCSs as indicators of a possibly sensitive dependence of measurements on where and when exactly they were taken. The analysis is based on offline drift simulations using German Bight surface layer currents obtained from archived output of the operational 3D baroclinic model BSHcmod, run operationally by the German Federal Maritime and Hydrographic Agency (BSH). The study aims for an assessment of the situations at specific times of interest rather than for a generic characterization or classification of given locations. Highly variable transport
75 paths in the German Bight area for the most part arise from residual currents being driven by changing wind conditions (Schrum, 1997; Callies et al., 2017a). Establishing a simple interrelationship between winds and overall finite-time transports is hardly possible, tracer trajectories aggregate the effects of possibly very different winds. Detailed numerical simulations, however, properly integrate such variable hydrodynamic transports during a specific observation period.

Hadjighasem et al. (2017) compare twelve candidate approaches that could be used for the identification of LCSs. Among
80 those, calculation of finite-time Lyapunov exponents (FTLE) is one of the most common methods. It is closely related to the finite-scale Lyapunov exponent (FSLE), originally introduced by Aurell et al. (1996, 1997) and used in experiments for diagnosing scale dependent separation rates between drifter pairs (LaCasce and Ohlmann, 2003; Sansón et al., 2017). Karrasch and Haller (2013), however, report some limitations for FSLE in LCS detection, suggesting that an approach based on FTLE distributions may be more reliable. The FTLE fields are independent of an observer's reference frame (Haller, 2015), representing
85 the rate at which neighbouring tracers ~~diverge-separate~~ according to the largest eigenvalue of the so-called Cauchy-Green strain tensor. ~~Ridges in the FTLE field are indicators of LCSs.~~

Building on work by Haller (2001), Shadden et al. (2005) ~~even~~ define LCS in terms of ~~these ridges, assuming that those approximately act as transport barriers. In two dimensions~~ ridges in the FTLE field. In two dimensions, the LCSs are material lines transported with the flow :-

90 ~~Haller (2011) discusses examples and, in good approximation, acting as transport barriers. Haller (2011), discussing counterexamples~~
in which substantial material flows ~~crossing a FTLE ridge occur. It may also happen that a LCS does not produce cross~~ a FTLE
ridge ~~or that a LCS suggested by FTLE does not exist. Therefore Haller (2011) occurred,~~ developed a more sophisticated
variational ~~theory that also involves the eigenvectors of the Cauchy-Green strain tensor. Farazmand and Haller (2012) present~~
105 ~~on the specification of strainlines along which exponential stretching occurs (to be distinguished from simple shear) applications.~~
Recently Tian et al. (2019) applied a variational method to identify the outer bounds of the Kuroshio current system.

~~Wiggins (2005) makes reservations that, as contrasted with many engineering applications, the presence and interaction of~~
~~very different scales in geophysical flows can restrict the possibility of simulating detailed particle drift paths. The present~~
~~study will therefore adhere to the simple conventional FTLE analysis. German Bight residual currents change with changing~~
100 ~~atmospheric winds (Schrum, 1997; Callies et al., 2017a) so that a description of exchange processes in a quasi-persistent hydrodynamic~~
~~space-time structure like gyres or jets (Wiggins, 2005) is not the topic here. Analysing surface transports simulated by the~~
~~operational hydrodynamic model BSHemod, FTLE fields will be compared with statistical measures like single-particle absolute~~
~~and two-particle relative dispersion, but also with the Lagrangian divergence (the average divergence that tracers experience~~
~~along their trajectories (Huntley et al., 2015)). It turns out that all these parameters deliver very consistent results~~
105 ~~Here, the~~
~~analysis will adhere to conventional FTLE fields.~~

The paper is organized as follows: Section 2 first describes the study area and how Lagrangian drift simulations were
performed based on pre-calculated hydrodynamic surface current fields. It follows a short compilation of the definitions of
the FTLE, Lagrangian divergence and statistical measures of dispersion. Presenting a couple of structures that emerged under
different wind conditions, Section 3 then ~~reports three prototypical situations, evaluated also with regard to fields of sea surface~~
110 ~~temperature and salinity tries to give an overview of the type of LCSs that can be found in the German Bight area.~~ Example
trajectories ~~illustrate~~ substantiate the relevance of FTLE ridges as material separatrices. ~~Three snapshots from a video available~~
~~in the supplement illustrate the temporal variability of LCSs.~~ A general discussion and a short summary conclude the paper.

2 Material and methods

2.1 Study area

115 The North Sea is a semi-enclosed shelf sea that connects to the north-eastern Atlantic at its northern boundary and through the
English Channel at its southwest (Sündermann and Pohlmann, 2011). Strong tidal forcing occurs as a co-oscillation triggered
by Atlantic tidal waves. This study focusses on the German Bight, the shallow south-eastern part of the North Sea (here: east
of 6.5°E and south of 56°N) with water depths of mainly ~~20-40 m~~ 20-50 m (see Fig. 1), adjoining the Dutch, the German
and the Danish coasts (Becker et al., 1992). In the German Bight, a mean cyclonic North Sea circulation corresponds with
120 residual currents from the southwest to the north. Superimposed to this mean circulation, a strong weather driven variability
occurs on short time scales (Schrum, 1997; Callies et al., 2017a). A fresh water plume emerging from the Elbe River and, to a

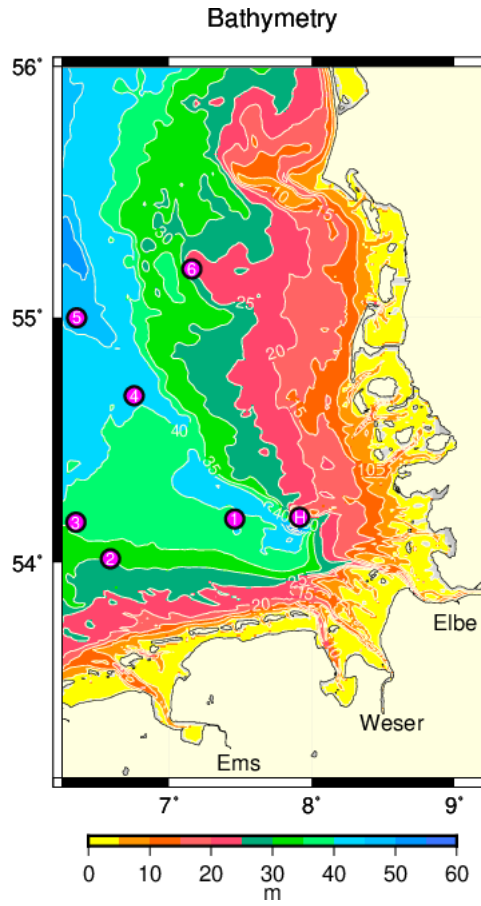


Figure 1. German Bight bathymetry. Magenta coloured circles indicate locations of six stations of the MARNET monitoring network (labels 1-6) and of the island of Helgoland (label H).

minor extent, also the Weser ~~river~~ (see Fig. 2) and the Ems rivers can be observed as a permanent feature. Transient eddies and meanders depend on bottom topography, baroclinic instabilities and wind effects.

The most important topographic feature is the old Elbe Glacial Valley, opening from today's Elbe estuary towards the northwest (~~west of Helgoland~~) into the open North Sea (see Fig. 1). Becker et al. (1992) summarize different types of fronts (river plume, thermal and upwelling fronts) that occur in the German Bight. Frontal structures depend on season but vary also on a short term basis (Budéus, 1989; Schrum, 1997). In the warm season, strong stratification occurs at water depths greater than approximately 30 m, mainly in the Elbe Glacial Valley. A baroclinic tidal mixing front (James, 1984; Holt and Umlauf, 2008) separates this region from the well-mixed more shallow coastal water, where stratification is prevented by strong tidal mixing (Krause et al., 1986).

2.2 Hydrodynamic fields

~~Offline drift simulations were based on surface currents~~ Surface layer currents used for offline drift simulations (see Section 2.3) as well as temperature fields were taken from archived BSHcmod model output. ~~Fields of surface temperature and salinity were taken from the same data base. BSHcmod~~ BSHcmod is a three-dimensional baroclinic circulation model, formulated using geographical coordinates and a flexible vertical resolution that allows for weakly inclined coordinate surfaces (Dick et al., 2008) of up to 36 layers. The model is run operationally by the Federal Maritime and Hydrographic Agency (BSH). ~~The model covers~~ since many years, providing the basis for different oceanographic services including search-and-rescue applications. It covers both the North Sea and the Baltic Sea and is two-way nested with approximately 900 m resolution in the German Bight area (Fig. 1) and approximately 5 km in the open North Sea (Dick et al., 2001). ~~In the vertical, a dynamical coordinate is used~~ ~~(Dick et al., 2008)~~ The domain of the present analysis roughly agrees with the region of 900 m resolution in German North Sea coastal waters.

In BSHcmod, advection and diffusion are calculated using a flux-corrected transport scheme. The hydrostatic and the Boussinesq approximations are applied. The Smagorinsky scheme (Smagorinsky, 1963) is used for the parameterization of horizontal viscosity. For an inclusion of wind stress, the parametrization by Smith and Banke (1975) is used. Stokes drift remains disregarded in the operational model output. The model's atmospheric forcing ~~on an hourly basis~~ is provided by the regional model COSMO-EU (Consortium for Small-Scale Modelling; Schulz and Schättler (2014)), run by the German Meteorological Service (Deutscher Wetterdienst – DWD). ~~For an inclusion of wind stress, the parametrization by Smith and Banke (1975) is used. Stokes drift remains disregarded in archived operational model output~~ The Swedish Meteorological and Hydrological Institute (SMHI) and the Federal Institute of Hydrology (BfG) provide runoff data for all major rivers that flow into the North Sea.

In the process of archiving, BSHcmod hydrodynamic fields with originally higher vertical resolution were re-gridded. Conserving transport rates, this was done in such a way that the ~~stored archived~~ surface currents used in this study ~~approximately represent~~ are representative for the uppermost 5 metres of the water column. ~~With drift simulations based on these currents plus a leeway of 0.6 % of wind in 10 m height, Callies et al. (2017b, 2019) reproduced observed drifter trajectories reasonably well.~~

2.3 Lagrangian drift simulations

~~Drift~~ Offline drift simulations were performed using the Lagrangian transport program PELETS-2D (Callies et al., 2011), based on BSHcmod ~~model-output~~ surface layer currents, archived on a 15 min basis. Originally, the PELETS toolbox developed at Helmholtz-Zentrum Geesthacht was designed for its use with hydrodynamic currents on unstructured triangular grids. Current fields provided on a regular grid (like those from BSHcmod) must be preprocessed, splitting each rectangular grid cell into two triangles. ~~This~~, a transformation of grid topology that does not affect the information content of hydrodynamic fields.

All simulations in this study were produced using the fourth-order Cash Karp method (Press et al., 1992) that belongs to the Runge Kutta family of solvers. ~~It should be mentioned, however, that a~~ simple Euler forward scheme, however, used in other PELETS applications (e.g. Callies et al., 2011, 2017b, 2019) gave very similar results. The maximum time step is set to 15 min. Velocities are updated earlier if a tracer particle moves to another triangular grid cell.

2.4 Finite-time Lyapunov exponents (FTLE) ~~as indicators of Lagrangian coherent structures (LCS)~~

Definition of the FTLE is based on a consideration of Lagrangian flow motions. A flow map Φ ~~relates~~ maps particle locations \mathbf{x}_0 , where particles were seeded at time t_0 , ~~to~~ onto their destinations \mathbf{x} at later time $t = t_0 + \tau$:

$$\Phi_{t_0}^\tau(\mathbf{x}_0) = \mathbf{x}(t_0 + \tau; t_0, \mathbf{x}_0). \quad (1)$$

~~Taking the spatial gradient~~ $\nabla \Phi_{t_0}^\tau = \partial \mathbf{x}(t_0 + \tau; t_0, \mathbf{x}_0) / \partial \mathbf{x}_0$ The following deformation gradient describes material deformation,

$$\nabla \Phi_{t_0}^\tau(\mathbf{x}_0) = \begin{pmatrix} \frac{\partial x}{\partial x_0} & \frac{\partial x}{\partial y_0} \\ \frac{\partial y}{\partial x_0} & \frac{\partial y}{\partial y_0} \end{pmatrix}, \quad (2)$$

where $\mathbf{x} = (x, y)$. The deformation's Jacobian provides the ratio of the area A of a deformed quadrangle to the area A_0 of an infinitesimal square it has its origin in. In case of a finite size initial square and a non-linear flow, this ratio refers to a quadrangle that approximates the emerging distorted patch. Similarly, a linear map sends an initially small circle to an ellipse. The lengths of the image area's semi-axes are given by the deformation gradient's two singular values μ_1, μ_2 , whose product equals the Jacobian determinant:

$$\frac{A}{A_0} = \det(\nabla \Phi_{t_0}^\tau) = \mu_1 \mu_2. \quad (3)$$

From the above deformation gradient, one obtains the following Cauchy-Green strain or deformation tensor (e.g. Shadden et al., 2005; Haller, 2015):

$$C(\tau; t_0, \mathbf{x}_0) = [\nabla \Phi_{t_0}^\tau(\mathbf{x}_0)]^T \nabla \Phi_{t_0}^\tau(\mathbf{x}_0). \quad (4)$$

This two-dimensional ~~(in case of two-dimensional flows)~~ tensor is symmetric and positive definite, symmetric and positive-definite tensor has two eigenvalues $\lambda_1 = \mu_1^2$ and $\lambda_2 = \mu_2^2$. Definition of the finite-time Lyapunov exponent (FTLE) is based on its largest

eigenvalue λ_{max} : the tensor's larger eigenvalue λ_1 :

$$185 \quad \text{FTLE}(\tau; t_0, \underline{x} \underline{x}_0) = \frac{1}{|\tau|} \ln \sqrt{\lambda_{max}(C(\tau; t_0, \underline{x}_0))} \log \sqrt{\lambda_1} = \frac{1}{|\tau|} \log(\mu_1) . \quad (5)$$

The absolute value of integration time τ is used because integration of particle drift can be conducted either forward or backward in time. The geometric interpretation of the FTLE refers to the maximum separation rate of neighbouring particles. ~~Maximum separation among particles started on a small circle around location \underline{x}_0 occurs for those particles that end up along the largest principal axis of an ellipse that evolved from the initially circular structure (see Haller, 2015, his Fig. 4)~~
 190 ~~(Haller, 2015).~~

~~For the computation of FTLE fields~~ To compute FTLE fields numerically, a regular Cartesian grid of tracers was released. ~~Initial-, initial~~ locations with 1 km resolution ~~covered~~ covering the German Bight area east of 6.5°E and south of 56°N (165 vortices in the longitudinal and 310 vortices in the latitudinal direction). The corresponding 51150 trajectories were integrated 250 hours ~~backward~~ back in time ($\tau = -250$ h). To avoid the computational burden of four ~~additional~~ close-by
 195 auxiliary trajectories, finite-differencing ~~involved in FTLE specification~~ (Eq. (4)2) was performed ~~involving trajectories seeded at neighbouring locations of~~ based on neighbouring trajectories already seeded on the regular FTLE grid.

~~If~~ In view of the limited vertical resolution of archived BSHcmod currents, values of the deformation gradient (Eq. (2)) were
~~tagged as missing each time~~ at least one of the four tracer trajectories needed for ~~FTLE calculation reached the coastline, the~~
~~FTLE value was treated as missing. Corresponding its~~ discrete calculation encountered a water depth of less than 5 m sometime
 200 in the course of its integration. Resulting gaps in the ~~FTLE fields depend on prevailing~~ fields of FTLE and related quantities
change with variable atmospheric forcing. As BSHcmod covers the whole North Sea, no ~~such problem occurs~~ specific treatment
is needed for particles that cross the open boundaries of the FTLE grid.

2.5 ~~Finite-Domain Lagrangian Divergence (FDLD)~~ Distinction between divergence and stretch

An incompressible two-dimensional flow field preserves the area of a Lagrangian patch during arbitrary deformations. ~~In the~~
 205 ~~present study this is not the case as the~~ Here, however, two-dimensional surface currents being used were extracted from
~~3D hydrodynamic fields, allowing three-dimensional hydrodynamic fields that allow~~ for vertical exchange of water masses.
 Huntley et al. (2015) developed a concept that splits FTLE values into contributions that come from area-preserving stretching
and deformation on the one hand and ~~dilation~~ area changes on the other. ~~With the area of a deformed elliptical Lagrangian~~
~~patch being proportional to the product of the two eigenvalues λ_i of the Cauchy-Green strain tensor, Huntley et al. define a~~
 210 ~~dilation rate~~ Given the singular values $\mu_1 > \mu_2$ of the deformation gradient $\nabla \Phi_{t_0}^T(\underline{x}_0)$, Huntley et al. (2015) introduce the
following stretch rate Σ :

$$\Sigma = \frac{1}{|\tau|} \log \left(\frac{\mu_1}{\mu_2} \right) . \quad (6)$$

In addition, they introduce the following dilation rate Δ in a two-dimensional flow field as: that describes the transformation of a Lagrangian patch's initial area A_0 to an area A after integration time τ .

$$\Delta = \frac{1}{|\tau|} \log \left(\frac{A}{A_0} \right) = \frac{1}{|\tau|} \log (\mu_1 \mu_2) , \quad (7)$$

where Eq. (3) has been used. From Eq. (5) it follows that the separation rate represented by the FTLE can be decomposed in terms of the above two components:

$$\underline{\Delta}_{\text{FTLE}} = \frac{\ln(\lambda_1 \lambda_2)}{|\tau|} \frac{\Delta + \Sigma}{2} . \quad (8)$$

According to Huntley et al., this parameter equals Dilation rate Δ can be shown to equal the average Eulerian horizontal divergences experienced by a fluid parcel along its pathway (Huntley et al., 2015; Duran et al., 2018, supplement). From the material derivative

$$\frac{dA}{dt} = A \nabla \cdot \mathbf{v} , \quad (9)$$

it follows that

$$A(t) = A_0 \exp \left(\int_{t_0}^{t_0+\tau} \nabla \cdot \mathbf{v}(t', \mathbf{x}(t')) dt' \right) . \quad (10)$$

Hernández-Carrasco et al. (2018) refer to this integral parameter the patch area's change rate, derived from past Eulerian divergences, as the Finite-Domain Lagrangian Divergence (FDLD),

$$\text{FDLD} = \frac{1}{\tau} \frac{1}{|\tau|} \log \left(\frac{A}{A_0} \right) = \frac{1}{|\tau|} \int_{t_0}^{t_0+\tau} \nabla_{\underline{H}} \cdot \mathbf{v}(t', \mathbf{x}(t')) dt' . \quad (11)$$

and They demonstrate its potential for supporting the interpretation of satellite based observations of surface chlorophyll a patches.

Analytically, the FDLD from Eq. (11) equals the dilation rate Δ from Eq. (7). In the present study, FDLD values were calculated at all locations with valid FTLE values. however, Eulerian divergences needed for the numerical evaluation of Eq. (11) were computed based on a discretization using introducing auxiliary points at a 250 m distance. Velocities at these auxiliary locations were obtained by linear interpolation in the respective grid triangle. As a result of this approach, estimated FDLD fields have slightly higher resolution than Δ fields derived from deformation gradients specified on the basic 1 km FTLE grid.

2.6 Absolute and relative dispersion

Absolute and relative dispersion are statistical measures for analysing Lagrangian data. Generally, absolute dispersion is defined as the second moment of the single particle displacement PDF, i.e. the variance of particle displacements relative to their starting

position, ~~which~~. This measure must not be confused with cloud variance (LaCasce, 2008). Ensemble averaging could be
 240 performed with respect to either different locations or different realizations at some fixed location. Here, following Haller and
 Yuan (2000), the simpler density of absolute dispersion is considered, describing just a single particle's squared displacement
 from its release point:

$$a^2(\tau; t_0, \mathbf{x}_0) = |\mathbf{x}(t_0 + \tau; t_0, \mathbf{x}_0) - \mathbf{x}_0|^2 \quad (12)$$

By contrast, relative dispersion describes the mean square separation of particle pairs with nearby initial release points. Relative
 245 dispersion at each node of the FTLE grid will be calculated combining the information from four particle pairs,

$$D^2(\tau; t_0, \mathbf{x}_0) = \frac{1}{4} \sum_{i=1}^4 |\mathbf{x}(t_0 + \tau; t_0, \mathbf{x}_0) - \mathbf{x}(t_0 + \tau; t_0, \mathbf{x}_0 + \delta \mathbf{x}_i)|^2 \quad (13)$$

where $\delta \mathbf{x}_i$ denotes the distance vector between neighbouring nodes. For a comparison with FTLE and FDLT fields, the loga-
 rithm of absolute and relative dispersion is a reasonable choice. Exponential growth of pair separations indicates the presence
 of Lagrangian chaos dynamical systems theory deals with (Wiggins, 2005).

250 3 Results

3.1 Examples

~~The following examples are~~ A couple of examples will be given, intended to illustrate the occurrence and time variability of
 Lagrangian structures in German Bight surface currents. None of these structures are persistent, occurrence and specific details
 depend on the past evolution of environmental conditions. All figures contain wind roses that summarize wind conditions
 255 during the past 250 hours. A video provided in the supplement exemplifies the time evolution of FTLE fields in the course of
the year 2016.

3.0.1 First example

3.1 First example

Fig. 2a shows the FTLE field for simulations initialized on 12 June 2015 (13:00 UTC) and extending over 250 hours backward
 260 in time. The ~~scale was chosen to well visualize ridges of large values (negative logarithmic FTLE values have been plotted as~~
~~if they were zero). All locations that gave rise to trajectories hitting the coast were disregarded.~~

graph leaves blank all locations from where trajectories reached regions with water depths below 5 m. At the time ~~the plot~~
Fig. 2 refers to, the most prominent feature ~~of in~~ the FTLE field is a-an extended south-north running ridge ~~that separates~~
~~the region of interest more or less into two halves~~ of high FTLE values. Further west, a less pronounced parallel second ridge
 265 occurs which, however, tends to be split into three or four segments. Other more local and sometimes also weaker filamentary
 structures can be recognized. Intended to illustrate the physical relevance of the central FTLE-ridge, Fig. 2a includes three

groups of four 250 h backward trajectories, initialized in the wider neighbourhood of stations 1, 4 and 6 of the MARNET monitoring network¹. To facilitate orientation and comparison, locations of the six MARNET stations and the island of Helgoland (station H) will be indicated in all further figures.

270 The ~~two~~-experiment shown refers to a situation with calm conditions during the last three days, weak winds blowing from the north/northeast under the influence of a high pressure system centred further west. Vectors in the top right corner of Fig. 2a show simulated 10 m wind directions near MARNET station 4 during the past 250 hours at ten hourly intervals. Wind speeds are represented by a colour code. The wind vector at the time of the plot is edged in red, those during the last 50 hours are edged in black. Strong winds ($> 17\text{m/s}$) from south/southwest occurred on the second and third of June, i.e. at the end of
275 the 250 hours backward integration period. Another event with enhanced wind speeds ($< 10\text{ m/s}$) from the north/northwest occurred about 4-6 days before the time of the FTLE field being shown. In this period, wind directions changed from roughly southern to northern directions. Both the directional changes and the higher drift speeds at the end of the integration back in time can also be recognized from the example drift trajectories displayed in Fig. 2a.

Two pairs of hypothetical in situ ~~stations-observation points~~ (indicated by small circles, green and ~~red~~) ~~near MARNET~~
280 ~~stations 1 and 6~~ blue) were located on either side of the central FTLE ridge near MARNET stations 1 and 6. Trajectory end points are indicated by small diamonds. Simulations show a clear separation of ~~trajectories-emerging-backward trajectories~~ that emerge from different sides of the FTLE ridge. By contrast, trajectories started on the same side of the ridge (having same colour) remain close to each other. ~~Trajectory end points are indicated by small diamonds. The example~~ The example backward trajectories illustrate how even close by in situ observations may encounter water bodies with a much different
285 history. A complementary experiment considers four trajectories in the vicinity of MARNET station 4, with now all release points being located within the same ~~contiguous region~~ area of low FTLE values. In this case all trajectories stay close together or even further converge.

¹ Station names: Deutsche Bucht (1), FINO1 (2), Ems (3), Nordseeboje III (4), Nordseeboje II (5), FINO3 (6)

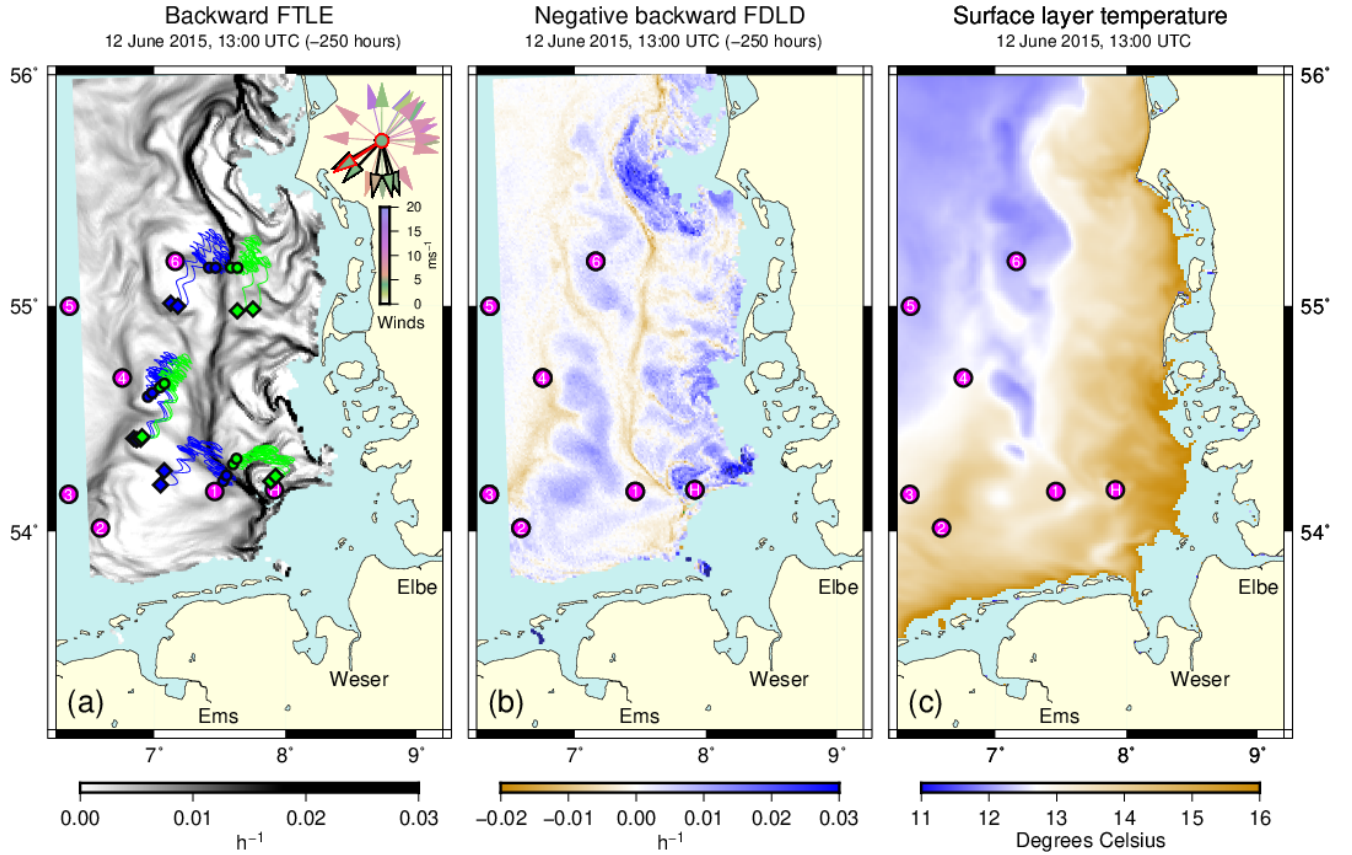


Figure 2. (a) FTLE field analysed for 12 June 2015 (13:00), [evaluating Eq. \(5\)](#) based on trajectories calculated 250 hours backward in time. [The scale was chosen to well visualize ridges of large values, negative values of the logarithmic FTLE have been plotted as if they were zero.](#) [Locations from where trajectories encountered a water depth of less than 5 m sometime in the course of their integration were disregarded.](#) Example backward trajectories are shown, using different colours [\(green/blue\)](#) for better distinction. Trajectory release points are indicated by circles, small diamonds mark trajectory end points. Labelled circles (magenta) indicate locations of six stations of the MARNET monitoring network [\(labels 1-6\)](#) and of the island of Helgoland [\(label H\)](#). [Vectors in the top right corner show past wind directions at ten hourly intervals, referring to conditions modelled for the location of MARNET station 4. Different wind speeds are represented by different colours. The wind vector at the time of the plot is edged in red, those during the last 50 hours are edged in black.](#) (b) Negative Lagrangian divergences (FDLD) calculated from Eq. (11) [for all pixels that also appear in panel \(a\). Values](#) [Few large positive values, exceeding the range covered by the colour scale map, are plotted in dark blue](#) [\(positive, occurs near the coast\) and dark green \(negative, very few points\).](#) (c) [Negative](#) [dilation rate \$\Delta\$, calculated according to Eq. Simulated mean temperatures in the uppermost 5](#) [\(?\) meters. To focus on open sea conditions, temperatures higher than 16°C are not shown.](#)

~~Divergence~~ Separation in backward time means ~~convergence~~ confluence in ordinary forward time. Therefore, the negative backward Lagrangian divergence FDL (see Eq. (11)) shown in Fig. 2b is to be read in agreement with the usual passage of time. ~~There is~~ Fig. 2b reveals a striking structural similarity with Fig. 2a. Water parcels located on backward FTLE ridges have predominantly experienced converging surface currents along their pathway during the last 250 hours. Between ~~these ridges~~ the ridges, there are wider regions with particles the history of which was dominated by ~~diverging~~ divergent Eulerian currents.

Studying the Agulhas current in the southwest Indian Ocean, van Sebille et al. (2018, their Fig. 3) found structures in fields of sea surface temperature (SST) that agreed with LCSs derived from geostrophic currents. For the present example, Fig. 2c shows the field of dilation rate Δ , calculated according to Eq. (??). In the open sea, dilation rates deliver the same spatial structure as the FDL a south-north oriented zone of relatively cool surface layer water, located in between narrow bands of higher temperature that tend to coincide with the FTLE ridges (Fig. 2a) and zones of convergence (Fig. 2b). The belt is made up by a couple of patches that bear a structural resemblance to patches of positive divergence in Fig. 2b, although the scale of values differs. This discrepancy in scale may be explained by numerical discretization and also the length of the integration interval which transforms small initial disks of the fluid into contorted structures rather than simple ellipses. More severe discrepancies occur near the coast, where even the signs of the analysed values differ. This deficiency presumably indicates that calculations based currents from a 5 m surface layer and with a 900 m horizontal resolution are inappropriate in these nearshore regions suggesting that some features of the temperature distribution in Fig. 2c can indeed be explained in terms of up- and downwelling simulated in the model. Meyerjürgens et al. (2020) found reduced relative dispersion for experimental drifters released in the vicinity of a tidal mixing front, indicating horizontal attraction in this region.

3.1.1 ~~Second example~~

3.2 Second example

~~Fig. 3a shows a situation (26 March 2018, 18:00) in which the b shows a~~ backward FTLE field that is even more clearly ~~partitioned~~ structured than the one in Fig. 2a, including also pronounced west-east oriented divides. ~~FTLE ridges are particularly sharp, so that the simulated origins of water bodies located on either side of a FTLE ridge vastly differ. Example tracer trajectories illustrate this effect, assuming~~ Note that FTLE ridges in the western part of the domain closely follow the bathymetric feature of the old Elbe Glacial Valley (see Fig. 1). Again, the origins of example tracers, estimated by backward trajectories with close by release points (red/green/blue) on either side of FTLE ridges, vastly differ. Particularly large differences between backward trajectories occur for the most northern and the most southern of the three pairs trajectories.

Similar to the example shown in Fig. 2, calm atmospheric conditions prevailed also for a couple of days preceding the time of Fig. 3b (26 March 2018, 18:00). Very strong easterly winds, however, persisted for a couple of days towards the end of the 250 h backward integration period (roughly 16-18 March). Nearly constant easterly wind directions for the last 50 hours can be distinguished from the wind rose in Fig. 3a, showing the FTLE field eight days earlier. Trajectories of North Sea drifters observed under these rare conditions (due to low temperatures in the UK called the 'Beast from the East') have been discussed by Stanev et al. (2019, see Fig. 3a therein). Some FTLE ridges that emerge according to Fig. 3a are aligned parallel with the

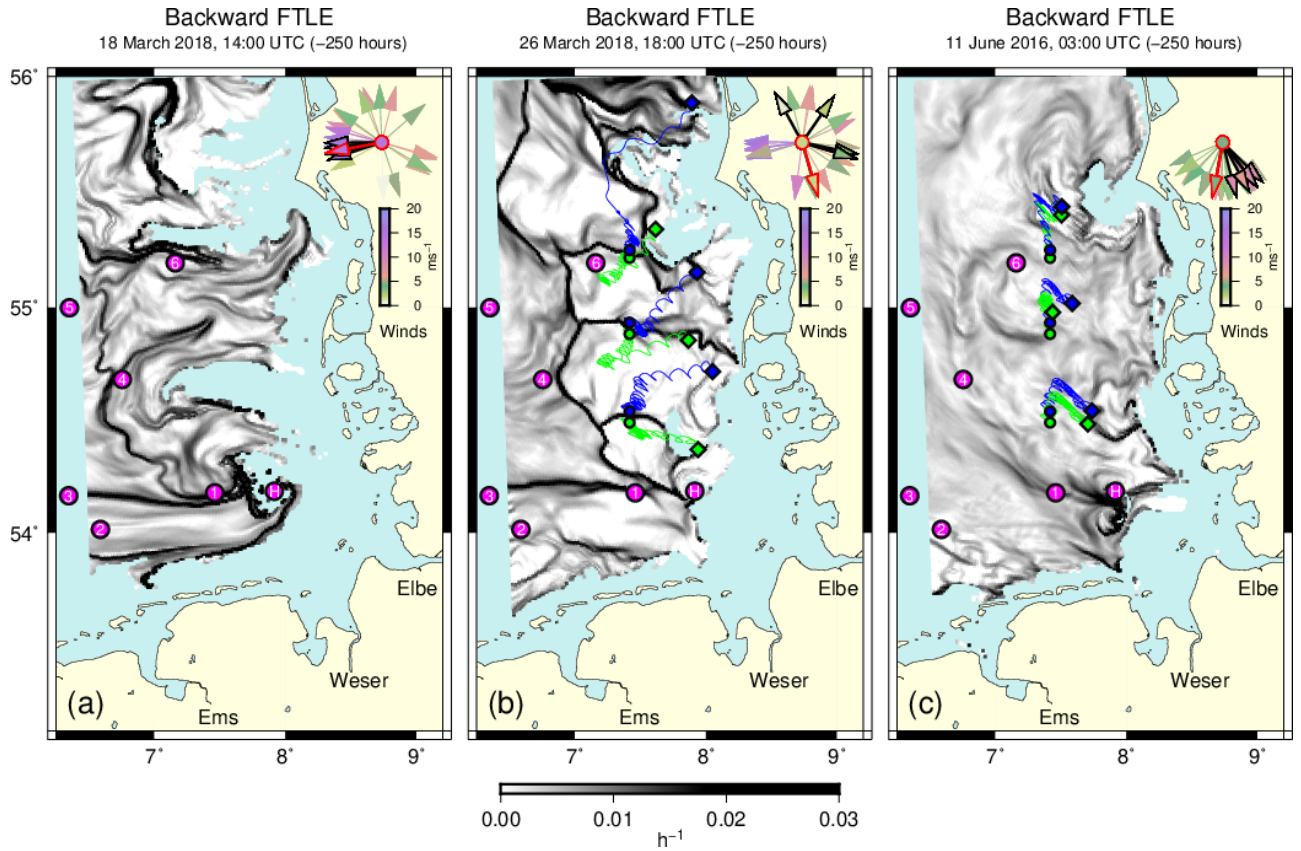


Figure 3. (a) Backward FTLE field (integration time 250 h) for 18 March 2018 (14:00). Magenta circles indicate locations of MARNET stations (1-6) and of the island of Helgoland (H). (b) Backward FTLE field about eight days later (26 March 2018, 18:00). Three pairs of example trajectories were started on either side (green/red blue), started on either side of FTLE ridges, are shown. Trajectory release points are indicated by circles, end points by diamonds. Magenta circles indicate locations of MARNET stations (1-6) and of the island of Helgoland (H). (c) Example of a much smoother backward FTLE field on 11 June 2016 (03:00). For the purposes of comparison, example backward trajectories were calculated from the same release points already used in panel (a). Vectors in the top right corner of each panel show past wind directions (modelled for the location of MARNET station 4) at ten hourly intervals. Different wind speeds are represented by different colours. Wind vectors at the times plots refer to are edged in red, those during the last 50 hours are edged in black.

easterly winds and seem to correspond with or to transform into sharp FTLE ridges in Fig. 3b under the subsequent much calmer conditions.

For comparison purposes, Fig. 3b-c shows the example of a much less structured FTLE field on 11 June 2016 (03:00) after persistently moderate winds from northerly directions. In this case sharp FTLE ridges are nearly absent. Overlaid to the FTLE field, the figure includes Fig. 3c includes direct counterparts of the trajectories shown in Fig. 3ab, released at exactly the same locations but on 11 June 2016 (10:00) rather than 26 March 2018 (18:00). Contrary to the situation in Fig. 3ab, now all neighbouring trajectories closely resemble each other, just being are very much alike, mainly shifted in agreement with shifted the slightly different release points. A similar behaviour occurs also at the time of Fig. 3a, if b when particles are released from the interior of a contiguous area delineated by the away from the FTLE ridges (see Fig. S1 in the supplement).

3.2.1 Third example

3.3 Third example

~~The third example, referring to~~

29 February 2016 (11:00), provides an analysis Fig. 4a) provides another example of weak winds that follow more stormy conditions. At about 26 February, strong winds to the south of an atmospheric low make way for weaker winds under the influence of a high pressure system. Different from the previous example, however, the strong winds some days ago persistently blew from the west rather than from the east. Again a net of sharp FTLE ridges can be observed in Fig. 4a.

Figs. 4b and 4c analyse the situation in terms of statistical dispersion measures. Fig. 4a-b displays the spatial distribution of absolute dispersion. Remember that each Each pixel in the plot is calculated based on just one trajectory and represents the squared distance between the corresponding trajectory's release and end point. The plot reveals some sharp demarcations between zones with either broadly similar or at least most smoothly changing drift velocities.

A measure that directly concentrates on small scale changes in drift behaviour is two-particle relative dispersion (Fig. 4b)-Maps c). Its distribution closely resembles the FTLE field in Fig. 4a. Also the two maps of absolute and relative dispersion are in very good agreement, relative dispersion highlighting sharp transitions in the graph of absolute dispersion. The two plots include the same

Fig. 4b also includes some example trajectories. Two test-Test trajectories near the horizontal divide south of MARNET station 4 illustrate a stepwise change of advection speed, giving rise to the enhanced level of absolute dispersion for the test station located more to the south (green). Note that a pure change of drift direction, maintaining advection speed, would have affected relative but not absolute dispersion. Three additional magenta trajectories, seeded at MARNET stations 1, 2 and 6, were included to just visualize spatial variability of transports.

Finally, it is to be noted that the relative dispersion graph in Fig. 4b closely resembles the backward FTLE field (Fig. S2). FTLE ridges subdivide the area of interest in the same way as relative dispersion does, differences can hardly be distinguished.

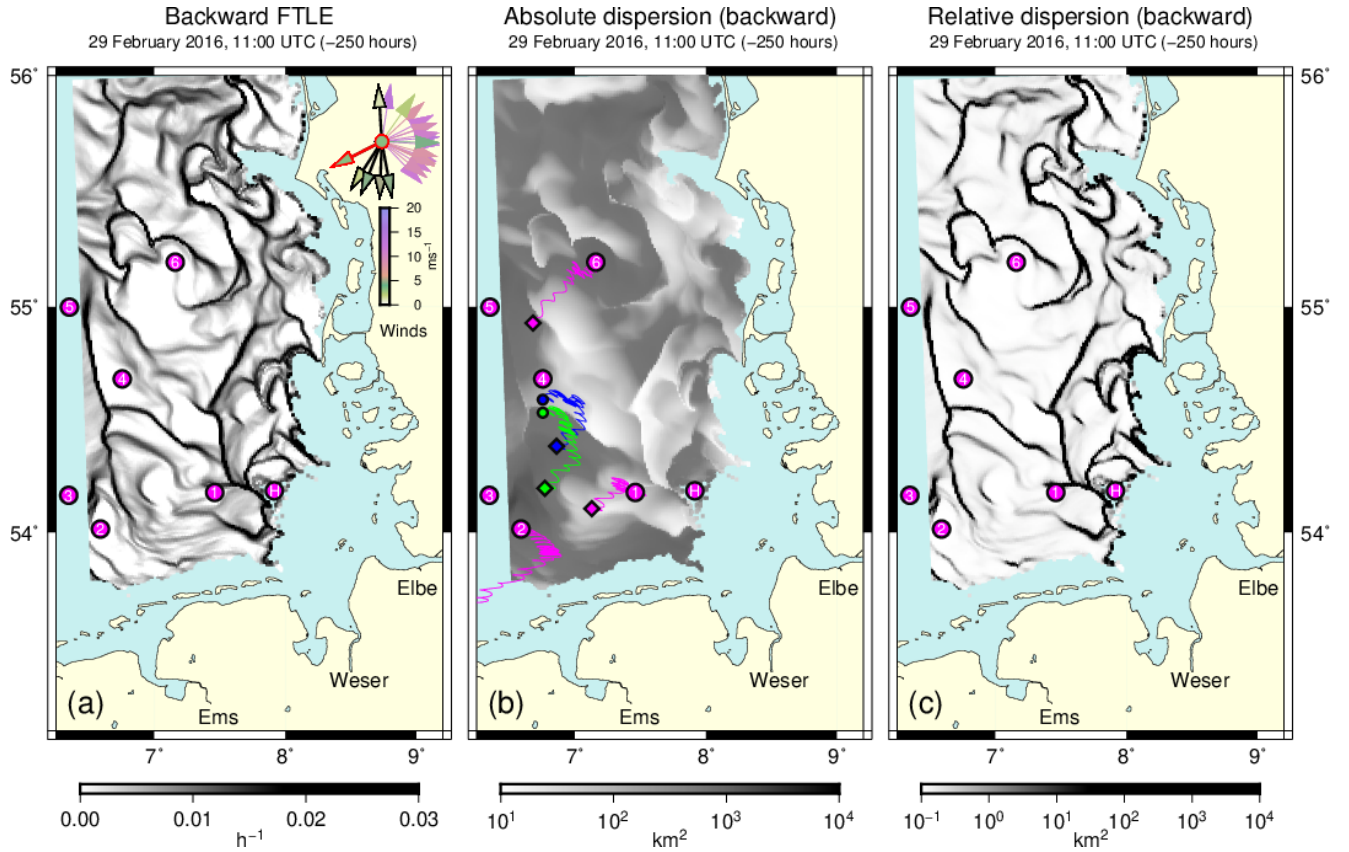


Figure 4. (a) Absolute dispersion-Backward FTLE field (squared-particle-displacements) for integration time 250 h backward-integrations started-on- for 29 Feb 2016 (11:00). Magenta circles indicate locations of MARNET stations (1-6) and of the island of Helgoland (H). Vectors in the top right corner show past wind directions (modelled for the location of station 4) at ten hourly intervals. Different wind speeds are represented by a colour map. The wind vector at the time of the plot is edged in red, those during the last 50 hours are edged in black. (b) Absolute dispersion (backward squared particle displacements) for the same time. Example trajectories shown were initialized at MARNET monitoring stations 1, 2 and 6 (magenta) and at two locations (red-small circles in blue and green) neighbouring MARNET station 4 to its south. Small diamonds indicate each trajectory's final location. (b) (c) Distribution of relative dispersion for the same situation time.

3.4 Surface temperatures Fourth example

Studying the Agulhas current in the southwest Indian Ocean, van Sebille et al. (2018, their Fig. 3) found structures in fields of sea surface temperature (SST) that agreed with LCSs derived from geostrophic currents. For the German Bight region, Meyerjürgens et al. (2020) found reduced relative dispersion for experimental drifters released in the vicinity of a tidal mixing front, indicating horizontal convergence in this region. This section addresses relationships between SST simulated in BSHemod and the LCSs presented in the above examples.

Sea surface temperatures at times the FTLE fields in Fig. 2 (a), Fig. 3a (b) and the distributions of absolute and relative dispersion in Fig. 4 (c) refer to:

Fig. ??a, referring to the situation in Fig. 2, shows a south-north oriented zone of relatively cool water. This belt is made up by a couple of patches that bear a striking structural resemblance to patches of positive divergence in Fig. 2b. These patches and the overall belt are delimited by the FTLE ridges shown in Fig. 2a. In the temperature field these lines of convergence (Fig. 2b) appear as being relatively warm. Fig. 2b suggests that some features of the temperature distribution in Fig. ??a can indeed be explained in terms of up- and downwelling.

Similar effects occur on 26 March 2018 (Fig. ??b, corresponding with Fig. 3a). The sharp west-east oriented ridges in Fig. 3a reappear in Fig. ??b as lines of relatively warm water (e.g. near MARNET station 6 or between MARNET stations 1 and 3). On the other hand, three tongues of relatively cool water extend westward from the coast into the areas between the lines of converging surface currents. Note that the eye-catching pronounced westward transition towards generally higher temperatures in the open sea (a transition broadly corresponding with increasing water depth towards the old Elbe Glacial Valley) does actually not always coincide with the main FTLE ridge neighbouring MARNET station 4. In particular to the north of this station, the FTLE ridge produces a line of relatively warm water that is clearly separate and shifted eastward (Fig. ??b).

Fig. ??c, showing the temperature field for 29 February 2016, corresponds with dispersion rates in Fig. 4. In this case, sharp transitions in the temperature field correspond with lines of large relative backward dispersion (Fig. 4b) or backward FTLE ridges (Fig. S2).

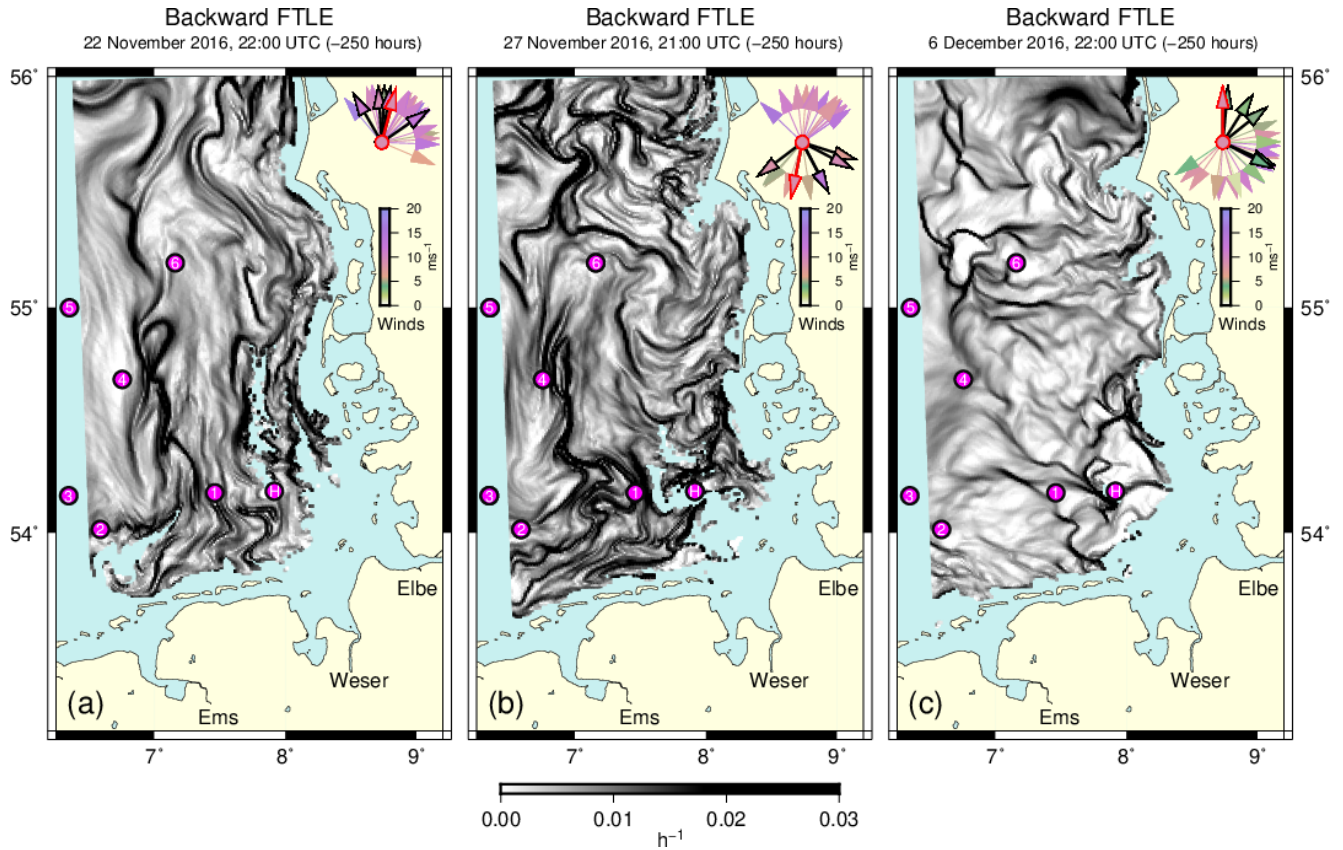
For all three examples addressed in Fig. ??, some related structures can be identified also in salinity fields (see Fig. S3). See Krause et al. (1986) and Budéus (1989) for a report on observations regarding the roles of temperature and salinity in different kinds of German Bight frontal structures.

3.5 Time evolution of coherent structures

FTLE (or dispersion) fields change continuously under changing environmental conditions. A video in the supplement, based on one FTLE field every 7 hours, shows the variability of FTLE ridges in the year throughout 2016. The three panels of Fig. 5 were extracted from this video. They illustrate the development within the almost three week period 23 November to 12 December. Long FTLE ridges aligned in a meridional direction (two week period 22 November to 6 December 2016, Fig. 5a) evolve into a more cellular structure (Fig. 5c).

385 shows the situation after 10 days of mostly strong winds from between southeast and west. The FTLE field ~~in Fig. 5b~~ is much less compartmentalized than the fields in Figs. 3a and 4b, for instance. Instead ~~, it contains more filamentary ridges that sometimes come very close. To illustrate the relevance of such narrow filaments, it shows long FTLE ridges aligned in a meridional direction, resembling the situation in Fig. 5b~~ combines a simulated backward trajectory starting at MARNET station 4 with another two trajectories (red and green) initialized slightly further east. Between the three seeding positions, FTLE
390 ~~ridges indicate enhanced backward particle separation (i.e. convergence in forward mode). Accordingly, the three trajectories end points are clearly much more separated from each other than tracers were at the outset. All three trajectories clearly reflect~~ 2a. On 23 November, winds change from southern winds to winds from northern directions. This entails a reversal of the ~~residual circulation that occurred during 22-24 November, when a pronounced cyclonic circulation changed formerly pronounced cyclonic~~ to an anticyclonic marine residual circulation². ~~However, the more the observation position is shifted to~~
395 ~~the east, the more any hypothetical measurements would reflect condition~~ the probed water parcel experienced further south. The wind rose in Fig. 5b (27 November, 21:00) clearly clusters strong winds from the south underlying the period covered by FTLEs in Fig. 5a and winds from the north more recently. It can be seen how this transition of winds generates structures including also more east-west oriented ridges. After 3 December, a high pressure area with very low winds extends into the North Sea region. Under such calm conditions, the FTLE field in Fig. 5c suggests evolution towards a more cellular structure.

²see https://www.bsh.de/DE/DATEN/Stroemungen/Zirkulationskalender/zirkulationskalender_node.html



Taking a monitoring perspective, this study focussed on ~~an~~the analysis of attracting LCSs, technically identified as repelling LCSs in backward simulations. ~~LCSs help delineate regions in situ observations are possibly representative for. A structure like the one shown in Fig. 2a, for instance, provides a warning that in the vicinity of the central south-north oriented FTLE ridge, even~~ Drift simulations based on BSHcmod surface layer currents revealed a pronounced time variability of LCSs, driven by ~~the recent history of wind conditions. Some LCSs, identified as ridges in the FTLE field, were found to be surprisingly sharp (e.g. Figs. 3b or 4a), so that~~ measurements at neighbouring locations might see water bodies with very different backgrounds. ~~In Fig. 3a the FTLE ridges are surprisingly sharp, so that in this case~~ Similarly, at a given station, even a small ~~relocation of a measurement site~~ wind-induced displacement of the FTLE field could substantially shift the ~~origin~~origin of water bodies being probed. ~~Convergence of water bodies with different past histories introduces uncertainties in the interpretation of~~ Being ~~aware of such sensitivities can be relevant for a proper interpretation of observational~~ data. Ridges in the simulated backward FTLE field convey ~~information on this uncertainty~~the information in a clear and amenable way.

~~Attracting LCSs, in dynamical systems theory also called unstable because of a fast stretching of particles along them (according to Harrison and Glatzmaier, 2010, an unfortunate historical definition), have been used for optimizing drifter deployments in field studies. Poje et al. (2002) proposed drifter deployment into attracting LCSs to ensure fast dispersal based on near-exponential material stretching, which lets drifters explore regions of high kinetic energy. Moleard et al. (2006) used this approach for assimilating drifter velocities into a ocean general circulation model. Different from these studies, Shadden et al. (2009) focus on repelling LCSs. Seeding drifters in a less localized way, Shadden et al. try to make drifters stay as long as possible in a specific region delineated by transport barriers.~~

~~The general idea followed here differs from the objective of Ricker and Stanev (2020), for instance, who aimed at the identification of mean particle accumulation patterns (in forward mode) in the European northwest shelf on time scales of months or years. In the light of time-dependent, sometimes narrow FTLE ridges, the general characterization of monitoring stations in terms of their areas of influence seems difficult to achieve. Duran et al. (2018) derived climatological LCSs (cLCS) based on low-pass filtered velocity fields. These cLCSs could then successfully be applied for a description of quasi-steady transport patterns in the Gulf of Mexico. Marine currents in the German Bight area, however, are much more variable. Therefore, this study suggests the use of detailed numerical simulations to classify probed water bodies with regard to their~~ presumable source regions. Similarly, detailed transport modelling could support the effective organization of field experiments. Not looking into the future, backward FTLE fields can be simulated already at the time when observations are actually taken. ~~Shadden et al. (2009) exemplify that a LCS's robustness might enable extrapolation of its separatrix function even beyond the time horizon of detailed operational hydrodynamic predictions, e.g. three days. Timely~~ Such timely model based information on ~~LCSs~~existing LCSs would allow for an adjustment of field campaigns to prevailing environmental conditions ~~and data already gathered. New data should complement rather than duplicate information already available. Proper interpretation of measurements can much depend on both location and time when observations were taken. This is analogous to what Lekien et al. (2005) found in forward mode, trying to optimize a pollution release scheme based on forward FTLE fields. In this~~

case favourable and unfavourable time spans for pollution release could clearly be distinguished from each other. Favourable
435 time windows might also be identified when taking observations.

In this study, FTLE fields were analysed on a grid with 1 km resolution, nearly matching resolution of the underlying
hydrodynamic current fields. Generally, defining FTLE fields on a finer grid to look at structures smaller than the resolution
of the Eulerian hydrodynamic model would have been possible (see Huhn et al., 2012, for instance). Generated by chaotic
advection with exponential material stretching rates, small scale structures arise from tracer simulations over distances much
440 exceeding numerical grid resolution (Huhn et al., 2012). Generally, Harrison and Glatzmaier (2010) found locations of major
LCSs to be fairly robust to spatial resolution in the light of the data already gathered.

According to Lekien et al. (2005), the relevance of FTLE ridges may be classified with regard to their length rather than
the size of FTLE values. Here, LCSs often turned out to have considerable length and to be connected, sometimes forming a
whole network. Examples shown suggest that in particular strong wind conditions trigger the occurrence of pronounced FTLE
445 ridges, often being of considerable length or demarcating a net of closed subregions. ~~Throughout the~~ These ridges continue
to exist for some time also under subsequent calmer wind conditions (e.g. Figs. 3a and 3b). Throughout this study, all FTLE
values were calculated based on trajectories integrated 250 hours back in time. This ~~is roughly ten times the integration time~~
~~Huhn et al. (2012) chose~~ integration time is much longer than just few tidal cycles which, for instance, Orre et al. (2006) chose
for analysing topographically constrained currents in a Norwegian fjord. Huhn et al. (2012) chose 24 hours for their study in
450 the Ria de Vigo estuary ~~in Spain~~. ~~Experiments reducing integration time to just~~, thereby preventing particles from reaching
the boundaries. In the present study, all trajectories that met water depths below 5 m were discarded. The long integration
time implied that even when being started under calm atmospheric conditions, trajectories experienced the storm event at
the end of their backward integration. A very interesting observations is, however, that with integration time being reduced
to just 50 or even 25 hours, revealed that hours, the key FTLE ridges tended to become less sharp but ~~to not change their~~
455 ~~locations (not shown)~~. This finding agrees with expectations (e.g. Peng and Dabiri, 2009; Shadden et al., 2009). According to
Peng and Dabiri (2009), in practice integration time should be chosen such that it makes LCSs well resolved and clearly
visible. As in Huhn et al. (2012), the tidal signal did not dominate the choice of integration time. The example trajectories
shown, illustrate how changing residual currents, driven by wind forcing, play a major role for particle separation. This is very
different in a Norwegian fjord, for instance, with topographically constrained currents driven mainly by tides (Orre et al., 2006)
460 :-

Branicki and Malek-Madani (2010) warn that conclusions from two-dimensional FTLE fields could be misleading in shallow
coastal waters with strong vertical mixing. Branicki and Malek-Madani see this point less critical when dealing with surface
currents and buoyant Lagrangian tracers. Tracer convergence (divergence in backward FTLE fields) near FTLE ridges did not
disappear (see Fig. S2, demonstrating that for the example shown in Fig. 3b). This finding is consistent with ~~an accumulation~~
465 of drifting material near tidal mixing fronts (Simpson and Pingree, 1978; Thiel et al., 2011). If two-dimensional current fields
are obtained from three-dimensional model output (as in this study), divergences may reflect injection of nutrients via vertical
transports. This provides important input for modelling chlorophyll *a* dynamics the fact that example backward trajectories in
Figs. 2a and 3b, for instance. ~~At the submesoscale, Hernández-Carraseo et al. (2018) found extreme divergence (indicating~~

upwelling) and convergence (indicating accumulation of surrounding phytoplankton standing stocks) both being associated with phytoplankton patches observed in coastal waters, show high drift velocities towards the end of the integration period but at the same time a clear separation of neighboured trajectories already right from the start. This proves a certain memory after the storm has ceased.

In this study, analysed structures were remarkably consistent for fields of FTLE, FDLD, dilation rate or measures of dispersion. Differences between the FTLE and FDLD fields discussed by Huntley et al. (2015) could not be seen on the spatial scale considered. Fields of path-averaged finite-time Lagrangian divergence FDLD corroborate the role of backward FTLE ridges as lines of convergence (see Fig. 2). This relationship agrees with the results of many oceanographic studies. Olascoaga et al. (2013, 2014), for instance, provide an example of how a chlorophyll *a* plume FTLE fields were analysed on a 1 km grid, nearly matching resolution of the marine current fields. Computationally more demanding FTLE analyses on a finer grid would have enabled identification of structures even smaller than resolution of the Eulerian hydrodynamic model arising, however, from tracer simulations over longer distances (Huhn et al., 2012). This shows that a classification of kinematic LCSs in terms of mesoscale or submesoscale features and processes may be difficult. Longer integration periods underlying the LCS analysis may filter more short-term features (Serra and Haller, 2016).

In their study of Lagrangian transports in the Gulf of Mexico coincides with an attracting LCS, Duran et al. (2018) found patterns shaping two-dimensional transports to arise from merely confluence, i.e. normal attraction and tangential stretching without convergence. Similarly, Lehahn et al. (2007) found satellite observations of chlorophyll filaments in the northeast Atlantic to well agree even with simulated geostrophic transports, contracting at and stretching along material lines. Referring to Lapeyre and Klein (2006), Lehahn et al. they argue that an ageostrophic secondary circulation injecting nutrients from deeper layers may trigger further chlorophyll production.

Combining SeaWiFS ocean colour data with altimetry-derived surface currents in the Brazil-Malvinas confluence zone, d'Ovidio et al. (2010) found that stirring by mesoscale currents can play an important role in structuring phytoplankton communities and even create what they call fluid dynamical niches, sharply delimited by LCSs. Hernández-Carrasco et al. (2018) study this topic at the submesoscale, using currents observed with High-Frequency Radar (HFR). Similarly, Olascoaga et al. (2013, their Fig. 1) provide an example of how a chlorophyll *a* plume in the Gulf of Mexico coincides with a divergence-free attracting LCS. At the smaller submesoscale, however, Hernández-Carrasco et al. (2018) found negative extremes of Lagrangian divergence to coincide with attracting LCSs identified as ridges in the field of backward Finite-Size Lyapunov Exponents (FSLE) analysed from HF radar data. Also in the present study, fields of path-averaged finite-domain Lagrangian divergence FDLD suggested the role of backward FTLE ridges as lines of convergence in coastal waters. According to Seales et al. (2018) attracting LCSs can also be targeted by fisheries, lead by lines of drifting foam or debris. However, Abraham and Bowen (2002), employing the FTLE for estimating a stirring rate from surface velocity data in This was explicitly shown for the example in Fig. 2 but pertains also to all the other examples.

Backward Jacobian determinant

26 March 2018, 18:00 UTC (-100 hours)

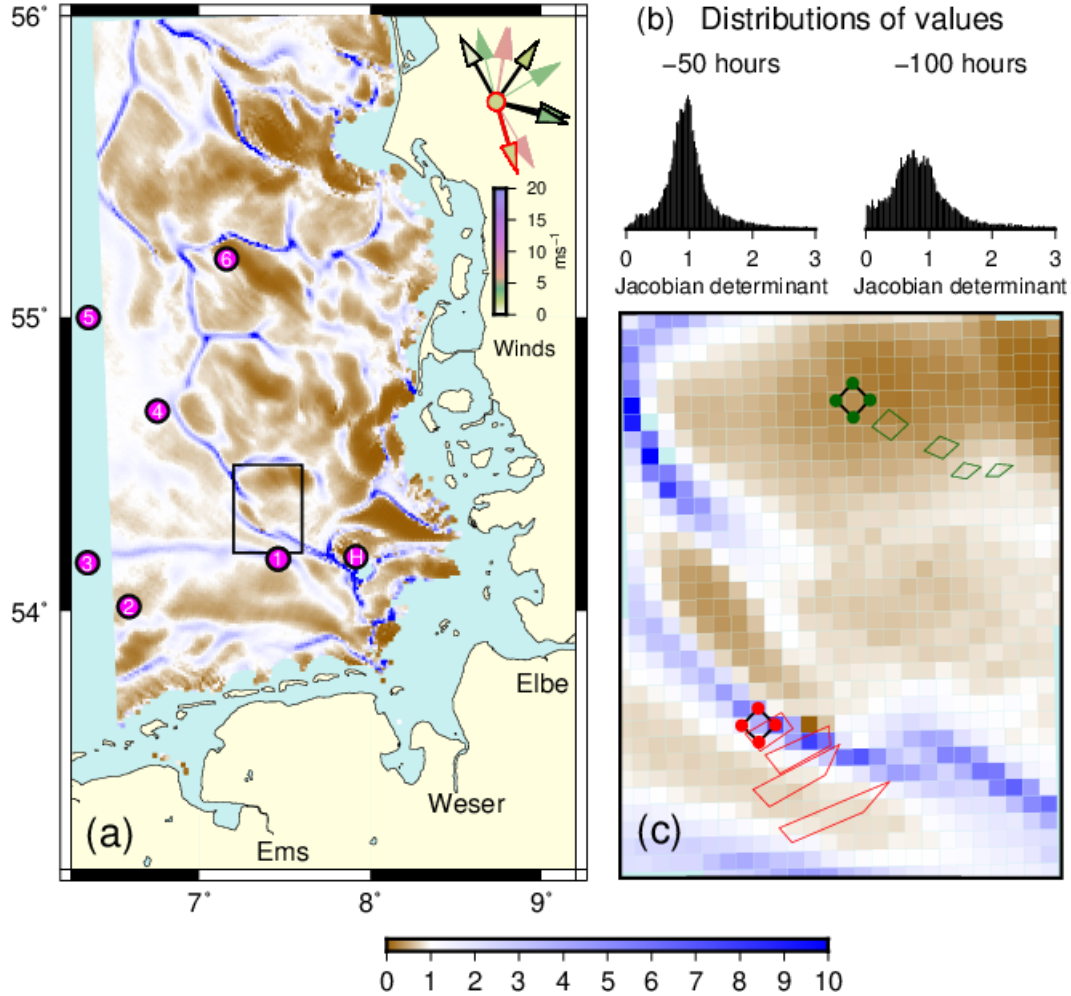


Figure 6. (a) Values of the Jacobian determinant (Eq. (4)) for 100 h backward simulations, initialized on 26 March 2018 (as in Fig. 3b). Few outliers exceeding the maximum value of the colour map were not specifically marked. Any negative values, possible due to finite initial distances, were omitted in the plot. Wind directions during integration time are shown at ten hourly intervals in the top right corner of the panel. The actual wind vector is edged in red, those during the last 50 hours are edged in black. (b) Histograms of Jacobian determinant values for integration times -50 h (left) and -100 h (right), respectively. Note that the distributions' flat tails extend beyond the ranges of values being shown. (c) Zooming in on the subregion indicated by the black frame in panel (a), the panel shows the time evolution of two square patches, corners of which are made up by the initial locations (red and green dots) of the four trajectories needed to calculate the discretized deformation gradient (Eq. (2)) at the respective square's center. Deformed quadrangles emerging during the -100 h integration period are shown at 25 hourly intervals. Factors of area in- or decreases $\mu_1\mu_2$ (Eq. (3)) are 1.56, 2.50, 3.40, 3.73 (red) and 0.96, 0.70, 0.42, 0.31 (green), where the last values equal the values for -100 h shown in the map. Corresponding stretches μ_1/μ_2 (see Eq. (6)) are 1.88, 3.01, 3.78, 5.52 (red) and 1.17, 1.52, 1.98, 2.36 (green).

Referring to the example addressed in Fig. 3b, Fig. 6a shows the corresponding field of the Jacobian determinant. A shorter integration period of only -100 h (rather than -250 h) was chosen to exclude the period of strong easterly winds that occurred about 8 days before the date of the analysis (compare the wind roses in Fig. 3b and Fig. 6a, respectively). Despite the shortened integration time, ridges in the backward Jacobian determinant field well coincide with FTLE ridges in Fig. 3b. Values of the Jacobian determinant are substantially spread around the neutral value of one that corresponds with zero divergence (Fig. 6b). Values further spread with increasing integration time. To exemplify patterns of transport, Fig. 6c shows the development of two patches with either increasing or decreasing area. At each time level, the quadrangles are defined by the positions of the four trajectories that emerge from the locations used to calculate the discretized deformation radius (Eq. (2)) in their centre. The more southern example emerges from a location on a ridge in the Jacobian determinant field. After 100 hours back in time, the initial area has grown by a factor of 3.73, which equals the values of the East-Australian-Current-region, emphasize that a model beyond a simple passive tracer concept would be needed to better understand chlorophyll distribution. determinant shown in the map. By contrast, starting from the more northern example location, the area decreases by a factor of 0.31. In both example cases the drift behaviour is far from being non-divergent.

Relatively stable FTLE ridges connected to the island of Helgoland, for instance, could also be relevant for sedimentation processes. However, again an analysis of ideal passive tracer trajectories is likely to be too simplistic for studying such effects. Movements of inertial tracers can substantially differ from those of fluid parcels. Therefore the idea of LCSs has been generalized to include dynamics of inertial particles (Sapsis and Haller, 2009; Sudharsan et al., 2016; Günther and Theisel, 2017). This theoretical concept has successfully been applied on the scale of ocean eddies (Beron-Vera et al., 2015) but also on the very small scale of jellyfish feeding (Peng and Dabiri, 2009; Sapsis et al., 2011).

In this study, drift simulations were not validated against data. However, it was shown that to some extent the LCSs identified in model output manifested themselves also in simulated fields of surface temperature (In both cases, however, also substantial stretching occurs. Final stretches μ_1/μ_2 of the example squares in Fig. ??) and salinity (Fig. S3) as intrinsic tracers. A relationship between frontal structures and FTLE ridges confirms the relevance of LCSs for surface current transports. Becker et al. (1992) summarize different types of fronts (river plume, thermal and upwelling fronts) that occur in the German Bight amount to 5.52 (red) and 2.36 (green). To differentiate the effects of divergent flows from divergence-free repulsion, Huntley et al. (2015) introduced the decomposition of the FTLE measure into dilation rate Δ and stretch rate Σ (see Section 2.5). For the three examples presented in Fig. 2, Fig. 3b and Fig. 4, respectively, Table 1 provides the correlations between FTLE and either dilation Δ or stretch rate Σ . In each case, correlations are given for the three different integration times of -50 h, -100 h and -250 h, respectively. Both correlations between FTLE and Δ or Σ are generally positive and of similar size, indicating that repulsion in the vicinity of backward FTLE ridges indeed occurs as a combination of divergence and stretching. In all three examples, an interesting observation is that the correlations between FTLE and dilation rate Δ increase with integration time, while correlations with stretch rate Σ decrease. As a result, correlation of FTLE values with dilation rate Δ is dominant for the -250 h integration time chosen in this study.

The temperature field in Fig. 2c provided an indication of confluent and possibly also convergent currents. Surface temperature observations by remote sensing might possibly provide a means to confirm simulated FDLD fields. Schrum (1997) showed how

Table 1. Correlations between FTLE and its additive components Δ and Σ (see Eq.8).

		<u>12 Jun 2015</u>	<u>26 Mar 2018</u>	<u>29 Feb 2016</u>
		<u>(Fig. 2)</u>	<u>(Fig.3b)</u>	<u>(Fig. 4)</u>
<u>corr (FTLE, Δ)</u>	<u>-50 h</u>	<u>0.41</u>	<u>0.59</u>	<u>0.68</u>
	<u>-100 h</u>	<u>0.51</u>	<u>0.66</u>	<u>0.73</u>
	<u>-250 h</u>	<u>0.65</u>	<u>0.72</u>	<u>0.77</u>
<u>corr (FTLE, Σ)</u>	<u>-50 h</u>	<u>0.69</u>	<u>0.63</u>	<u>0.57</u>
	<u>-100 h</u>	<u>0.65</u>	<u>0.57</u>	<u>0.47</u>
	<u>-250 h</u>	<u>0.52</u>	<u>0.50</u>	<u>0.37</u>

For three examples presented in this paper, the table shows correlations obtained for backward integration times τ =-50 h, -100 h and -250 h, respectively.

the spatial extent of thermohaline stratified areas, a precondition for the occurrence of tidal mixing fronts, depends on wind forcing ~~possibly inducing that~~ possibly induces differential advection. In a recent paper, Chegini et al. (2020) provided a more detailed analysis of different processes that affect stratification and destratification in the German Bight area, including freshwater buoyancy input. Location of the Elbe River plume again depends on the wind driven residual circulation. ~~Against this backdrop, it can be assumed that atmospheric forcing is also~~, which further substantiates the assumption of atmospheric forcing being a key driver for the generation, movement and extinction of German Bight LCSs.

~~Although some patterns in the temperature (and salinity) field seem clearly related to ridges in the FTLE fields, it must nevertheless be noted that there is no one-to-one relationship. An example for this provides the rather smooth FTLE field in Fig. 3b. The corresponding temperature field (Fig. S4a) shows small-scale structures with less clear counterparts in the FTLE field. According to Fig. S4b, the Lagrangian divergence FDLD reproduces structures seen in the temperature field, but FDLD values are clearly smaller than those in Fig. 3b. Combining pure flow dynamics with a simple representation of the dynamics of temperature itself might be necessary for an explanation of these structures in the temperature field (Abraham and Bowen, 2002). Note that large divergences in coastal regions are~~ Relatively persistent FTLE ridges related to the island of Helgoland, for instance, could possibly be relevant for sedimentation processes. However, movements of inertial tracers can substantially differ from those of fluid parcels, so that an analysis of ideal passive tracer trajectories is likely to be artefacts because of water depths in tidal waters falling below the depth of the assumed 5 m surface layer (remember the same type of discrepancies also between Figs. 2b and 2e) too simplistic in that context. The idea of LCSs has been generalized, however, to explicitly include the dynamics of inertial particles (Sapsis and Haller, 2009; Sudharsan et al., 2016; Günther and Theisel, 2017). This theoretical concept has successfully been applied on the scale of ocean eddies (Beron-Vera et al., 2015) but also on the very small scale of jellyfish feeding (Peng and Dabiri, 2009; Sapsis et al., 2011).

~~FTLE barriers may. Although numerical models can make observers aware of FTLE barriers that~~ move, disappear or newly arise under changing environmental conditions. ~~Numerical models are valuable tools for making observers aware of this fact. However, hydrodynamic models,~~ they can never provide a perfect surrogate nature. Guo et al. (2016) propose concepts to extend the conventional analysis of deterministic FTLE fields and ridges to uncertain flow conditions. In a comparative study, Hufnagl et al. (2017) found considerable discrepancies between the results from a large number of different North Sea tracer simulations essentially based on vertical mean currents. ~~For surface drift simulations, additional simulation errors may arise from the necessity to specify the extent to which near surface currents are exposed to wave related Stokes drift or a direct wind drag. In field studies, corresponding parameters may be tuned empirically (e.g. Callies et al., 2017b)~~ Wiggins (2005) makes reservations that, as contrasted with many engineering applications, the presence and interaction of very different scales in geophysical flows can restrict the possibility of simulating detailed particle drift paths. Altogether, simulated FTLE ~~distributions field~~ will always be imperfect. ~~Guo et al. (2016) propose concepts to extend the conventional analysis of deterministic FTLE fields and ridges to uncertain flow conditions.~~ However, even in case of inaccurate simulations, ~~the simulated FTLE would at least warn~~ simulated FTLE fields will warn users about key sensitivities of specific model output. If an observation is taken close to a simulated FTLE ridge, a simulated backward trajectory for this location must be used with due care.

This study did not address repelling LCSs in prediction ~~mode. However, it is obvious that the above difficulties also occur when forward simulations are~~ (forward) mode. Drift simulations are important tools employed for search and rescue ~~(Breivik et al., 2013)~~ (SAR), for instance. ~~A forward FTLE field could possibly warn users against particularly sensitive dependences on the assumed location of numerical drift simulations. In tracer experiments, substantial model data discrepancies could result from just a slight misspecification of initial locations or a moderate displacement of simulated LCSs relative to reality~~ (Breivik et al., 2013). Serra et al. (2020) proposed the use of objective Eulerian coherent structures (OECS) in this context, a concept developed by Serra and Haller (2016) for being used when quick operational decisions are to be made. According to Serra and Haller (2016), OECSs can be understood as short-time limits of LCSs, applicable for a time horizon of very few hours. More long-term forward simulations are feasible and can be afforded in the context of ecosystem hindcasts, analysing larval transport and dispersal, for instance.

For surface drift simulations, additional uncertainties may arise from the necessity to specify the extent to which near surface currents are exposed to a direct wind drag. Callies et al. (2017b, 2019) found that a successful simulation of observed drifter trajectories needed BSHcmod surface currents to be augmented by a leeway of 0.6 % of 10 m winds. Besides a small direct wind drag exerted on the drifters themselves, this leeway compensates for insufficient vertical resolution in the archived surface current fields (representing a layer of 5 m depth). In addition, the leeway may also parameterize wave related Stokes drift not being considered explicitly (Callies et al., 2017b; Sutherland et al., 2020). Example forward FTLE fields including a 6 % leeway are shown in Fig. S3. The example shows that FTLE ridges are modified but do not disappear when the smooth fields of a wind induced leeway are superimposed to marine currents. This conclusion directly translates to all the backward FTLE fields analysed in this paper.

The analysis of backward surface tracer simulations in the German Bight region revealed the intermittent presence of linear structures (LCSs) across which the past history of water bodies substantially changes. Such sensitive dependences of backward trajectories on tracer seeding positions, represented by narrow ridges in the ~~fields of either backward FTLE or backward relative dispersion are potential sources of uncertainty in the interpretation of in situ FTLE field~~, could entail differences between in situ
 595 observations even at neighbouring locations. Therefore, an evaluation of spatially distributed in situ observations could benefit from the awareness of changing FTLE fields, analysed based on either numerical simulations or possibly high frequency (HF) radar observational data.

In the presence of ~~repelling LCSs, large narrow~~ FTLE ridges, marked differences between observed and simulated tracer tra-
 jectories do not necessarily reflect poor model performance. If the location of a simulated LCS does not fully agree with reality,
 600 a tracer release point may come to lie on different sides of the ~~separatrix~~ separatrices in the model and in nature, respectively. In this case, a naive comparison of ~~emerging~~ trajectories could much exaggerate inconsistencies. The same arguments pertain to a comparison of different drift models. ~~Conventional~~ Therefore, conventional model evaluations based on individual drift paths might be ~~supplemented~~ complemented with a comparison of simulated FTLE fields ~~that highlight spatial variability of prediction uncertainty~~.

605 Examples illustrated the variability of ~~LCSs in the German Bight~~ German Bight surface layer LCSs under changing wind conditions. For a more comprehensive picture it ~~would~~ could be useful to establish a ~~link between the formal model that estimates the basic characteristics of backward FTLE fields, given a~~ recent history of atmospheric forcing, ~~tidal movements and the main characteristics of the backward FTLE fields to be expected~~. The examples studied suggest that model uncertainties occur particularly in the aftermath of storm conditions. Due to the presence of sometimes complex filamentary structures, a
 610 decomposition of FTLE fields in terms of a mean ~~field plus the sum of~~ plus a number of weighted anomaly fields (~~empirical orthogonal function analysis~~) seems not very promising. Classification of FTLE fields into a limited number of categories ~~might~~ could be useful. This problem is left to future research.

Code and data availability. The hydrodynamic data analysed in this paper were obtained from the repository of the Federal Maritime and Hydrographic Agency (BSH). For access to the archived results of the operational hydrodynamical model BSHcmod, please contact BSH
 615 (www.bsh.de). The Lagrangian drift code PELETS is available on request from the author.

Video supplement. A video is provided (FTLE_2016.avi) that demonstrates the temporal development of FTLE fields in the course of the year 2016, based on FTLE fields calculated every 7 hours.

Author contributions. The author performed all analyses and prepared the manuscript.

Competing interests. The author declares that he has no conflict of interest.

620 *Acknowledgements.* Drift simulations were based on BSHmod currents provided by the Federal Maritime and Hydrographic Agency (BSH).
Graphs were produced using the Generic Mapping Tools software (GMT) available from www.soest.hawaii.edu/gmt/. I would like to thank
Rodrigo Duran for some helpful suggestions. I furthermore appreciate comments by Jens Meyerjürgens and two anonymous referees.

References

- Abraham, E. R. and Bowen, M. M.: Chaotic stirring by a mesoscale surface-ocean flow, *Chaos*, 12, 373–381,
625 <https://doi.org/10.1063/1.1481615>, 2002.
- Aurell, E., Boffetta, G., Crisanti, A., Palatin, G., and Vulpiani, A.: Growth of noninfinitesimal perturbations in turbulence, *Phys. Rev. Lett.*,
77, 1262–1265, <https://doi.org/10.1103/PhysRevLett.77.1262>, 1996.
- Aurell, E., Boffetta, G., Crisanti, A., Palatin, G., and Vulpiani, A.: Predictability in the large: an extension of the concept of Lyapunov
exponent, *J. Phys. A*, 30, 1–26, <https://doi.org/10.1088/0305-4470/30/1/003>, 1997.
- 630 Baschek, B., Schroeder, F., Brix, H., Riethmüller, R., Badewien, T. H., Breitbach, G., Brügge, B., Colijn, F., Doerffer, R., Eschen-
bach, C., Friedrich, J., Fischer, P., Garthe, S., Horstmann, J., Krasemann, H., Metfies, K., Merckelbach, L., Ohle, N., Petersen, W.,
Pröfrock, D., Röttgers, R., Schlüter, M., Schulz, J., Schulz-Stellenfleth, J., Stanev, E., Staneva, J., Winter, C., Wirtz, K., Wollschläger,
J., Zielinski, O., and Ziemer, F.: The Coastal Observing System for Northern and Arctic Seas (COSYNA), *Ocean Sci.*, 13, 379–410,
<https://doi.org/10.5194/os-13-379-2017>, <https://www.ocean-sci.net/13/379/2017/>, 2017.
- 635 Becker, G. A., Dick, S., and Dippner, J. W.: Hydrography of the German Bight, *Mar. Ecol. Prog. Ser.*, 91, 9–18, 1992.
- Beron-Vera, F. J., Olascoaga, M. J., Haller, G., Farazmand, M., Triñanes, J., and Wang, Y.: Dissipative inertial transport patterns near coherent
Lagrangian eddies in the ocean, *Chaos*, 25, 087 412, <https://doi.org/10.1063/1.4928693>, 2015.
- Branicki, M. and Malek-Madani, R.: Lagrangian structure of flows in the Chesapeake Bay, *Nonlin Processes Geophys.*, 17, 149–168,
<https://doi.org/10.5194/npg-17-149-2010>, 2010.
- 640 Breivik, Ø., Allen, A. A., Maisondieu, C., and Olagon, M.: Advances in search and rescue at sea, *Ocean Dyn.*, 63, 83–88,
<https://doi.org/10.1007/s10236-012-0581-1>, 2013.
- Budéus, G.: Frontal variability in the German Bight, *Sci. Mar.*, 53, 175–185, 1989.
- Callies, U., Plüß, A., Kappenberg, J., and Kapitza, H.: Particle tracking in the Vicinity of Helgoland, North Sea: A Model Comparison, *Ocean
Dyn.*, 61, 2121–2139, <https://doi.org/10.1007/s10236-011-0474-8>, 2011.
- 645 Callies, U., Gaslikova, L., Kapitza, H., and Scharfe, M.: German Bight residual current variability on a daily basis: principal components of
multi-decadal barotropic simulations, *Geo-Mar. Lett.*, 37, 151–162, <https://doi.org/10.1007/s00367-016-0466-2>, 2017a.
- Callies, U., Groll, N., Horstmann, J., Kapitza, H., Klein, H., Maßmann, S., and Schwichtenberg, F.: Surface drifters in the German Bight:
model validation considering windage and Stokes drift, *Ocean Sci.*, 13, 799–827, <https://doi.org/10.5194/os-13-799-2017>, 2017b.
- Callies, U., Carrasco, R., Floeter, J., Horstmann, J., and Quante, M.: Submesoscale dispersion of surface drifters in a coastal sea near offshore
650 wind farms, *Ocean Sci.*, 15, 865–889, <https://doi.org/10.5194/os-15-865-2019>, 2019.
- Cegini, F., Holtermann, P., Kerimoglu, O., Becker, M., Kreus, M., Klingbeil, K., Gräwe, U., Winter, C., and Burchard, H.: Processes of
stratification and destratification during an extreme river discharge event in the German Bight ROFI, *J. Geophys. Res.: Oceans*, 125,
e2019JC015 987, <https://doi.org/10.1029/2019JC015987>, 2020.
- Chen, K., Ni, M., Cai, M., Huang, J. W. D., Chen, H., Wang, X., and Liu, M.: Optimization of a coastal environmental monitor-
655 ing network based on the Kriging method: A case study of Quanzhou Bay, China, *Biomed. Res. Int.*, 2016, Article ID 7137 310,
<https://doi.org/10.1155/2016/7137310>, 2016.
- Dick, S., Kleine, E., Müller-Navarra, S., Klein, H., and Komo, H.: The operational circulation model of BSH (BSHcmod). Model description
and validation, *Tech. Rep. 29/2001*, BSH, 2001.

- Dick, S., Kleine, E., and Janssen, F.: A new operational circulation model for the North Sea and Baltic Sea using a novel vertical co-
660 ordinate setup and first results, in: Coastal to Global Operational Oceanography: Achievements and Challenges. Proceedings of the Fifth
International Conference on EuroGOOS, 20-22 May 2008, Exeter, UK, edited by Dalhin, H., Bell, M. J., Flemming, N. C., and Petersen,
S. E., 2008.
- d'Ovidio, F., De Monte, S., Alvain, S., Dandonneau, Y., and Lévy, M.: Fluid dynamical niches of phytoplankton types, PNAS, 107, 18 366–
18 370, <https://doi.org/10.1073/pnas.1004620107>, 2010.
- 665 d'Ovidio, F., Penna, A. D., Trull, T. W., Nencioli, F., Pujol, M.-I., Rio, M.-H., Park, Y.-H., Cotté, C., Zhou, M., and Blain, S.: The biogeochem-
ical structuring role of horizontal stirring: Lagrangian perspectives on iron delivery downstream of the Kerguelen Plateau, Biogeosciences,
12, 5567–5581, <https://doi.org/10.5194/bg-12-5567-2015>, 2015.
- Duran, R., Beron-Vera, F. J., and Olascoaga, M. J.: Extracting quasi-steady Lagrangian transport patterns from the ocean circulation: An
application to the Gulf of Mexico, Scientific Reports, 8:5218, 9, <https://doi.org/10.1038/s41598-018-23121-y>, 2018.
- 670 Farazmand, M. and Haller, G.: Computing Lagrangian coherent structures from their variational theory, Chaos, 22, 013 128,
<https://doi.org/10.1063/1.3690153>, 2012.
- Günther, T. and Theisel, H.: Backward finite-time Lyapunov exponents in inertial flows, IEEE Trans. Vis. Comput. Graph., 23, 970–979,
<https://doi.org/10.1109/TVCG.2016.2599016>, 2017.
- Guo, H., He, W., Peterka, T., Shen, H.-W., Collis, S. M., and Helmus, J. J.: Finite-time Lyapunov exponents and Lagrangian coherent
675 structures in uncertain unsteady flows, IEEE Trans. Vis. Comput. Graph., 22, 1672–1682, <https://doi.org/10.1109/TVCG.2016.2534560>,
2016.
- Hadjighasem, A., Farazmand, M., Blazeviski, D., Froyland, G., and Haller, G.: A critical coparison of Lagrangian methods for coherent
structure detection, Chaos, 27, 053 104, <https://doi.org/10.1063/1.4982720>, 2017.
- Haller, G.: Distinguished material surfaces and coherent structures in three-dimensional fluid flows, Physica D, 149, 248–277,
680 [https://doi.org/10.1016/S0167-2789\(00\)00199-8](https://doi.org/10.1016/S0167-2789(00)00199-8), 2001.
- Haller, G.: A variational theory of hyperbolic Lagrangian coherent structures, Physica D, 240, 574–598,
<https://doi.org/10.1016/j.physd.2010.11.010>, 2011.
- Haller, G.: Lagrangian coherent structures, Annu. Rev. Fluid Mech., 47, 137–162, <https://doi.org/10.1146/annurev-fluid-010313-141322>,
2015.
- 685 Haller, G. and Yuan, G.: Lagrangian coherent structures and mixing in two-dimensional turbulence, Physica D, 147, 352–370,
[https://doi.org/10.1016/S0167-2789\(00\)00142-1](https://doi.org/10.1016/S0167-2789(00)00142-1), 2000.
- Harrison, C. S. and Glatzmaier, G. A.: Lagrangian coherent structures in the California Current System - sensitivities and limitations, Geophys.
Astro. Fluid Dyn., 106, 22–44, <https://doi.org/10.1080/03091929.2010.532793>, 2010.
- Hernández-Carrasco, I., Orfila, A., Rossi, V., and Garçon, V.: Effect of small scale transport processes on phytoplankton distribution in
690 coastal seas, Scientific Reports, 8, 8613, <https://doi.org/10.1038/s41598-018-26857-9>, 2018.
- Holt, J. and Umlauf, L.: Modelling the tidal mixing fronts and seasonal stratification of the Northwest European Continental shelf, Cont.
Shelf Res., 28, 887–903, <https://doi.org/10.1016/j.csr.2008.01.012>, 2008.
- Hufnagl, M., Payne, M., Lacroix, G., Bolle, L. J., Daewel, U., Dickey-Collas, M., Gerkema, T., Huret, M., Janssen, F., Kreuz, M., Pätsch,
J., Pohlmann, T., Ruardij, P., Schrum, C., Skogen, M. D., Tiessen, M. C., Petitgas, P., van Beek, J. K., van der Veer, H. W., and
695 Callies, U.: Variation that can be expected when using particle tracking models in connectivity studies, J. Sea Res., 127, 133–149,
<https://doi.org/10.1016/j.seares.2017.04.009>, 2017.

- Huhn, F., von Kameke, A., Allen-Perkins, S., Montero, P., Venancio, A., and Pérez-Muñuzuri, V.: Horizontal Lagrangian transport in a tidal-driven estuary - Transport barriers attached to prominent coastal boundaries, *Cont. Shelf Res.*, 39-40, 1–13, <https://doi.org/10.1016/j.csr.2012.03.005>, 2012.
- 700 Huntley, H. S., Lipphardt, B. L., Jacobs, G., and Kirwan Jr., A. D.: Clusters, deformation, and dilation: Diagnostics for material accumulation regions, *J. Geophys. Res.*, 120, 6622–6636, <https://doi.org/10.1002/2015JC011036>, 2015.
- James, I. D.: A three-dimensional numerical shelf-sea front model with variable eddy viscosity and diffusivity, *Cont. Shelf Res.*, 3, 69–98, 1984.
- Karrasch, D. and Haller, G.: Do finite-size Lyapunov exponents detect coherent structures?, *Chaos*, 23, 043126, <https://doi.org/10.1063/1.4837075>, 2013.
- 705 Kim, N.-H. and Hwang, J. H.: Optimal design of water quality monitoring networks in semi-enclosed estuaries, *Sensors*, 20, 1498, <https://doi.org/10.3390/s20051498>, 2020.
- Krause, G., Budeus, G., Gerdes, D., Schaumann, K., and Hesse, K.: Frontal systems in the German Bight and their physical and biological effects, in: *Marine Interfaces Ecohydrodynamics*, edited by Nihoul, J. C. J., pp. 119–140, Elsevier, Amsterdam, 1986.
- 710 LaCasce, J. H.: Statistics from Lagrangian observations, *Prog. Oceanogr.*, 77, 1–29, <https://doi.org/10.1016/j.pocean.2008.02.002>, 2008.
- LaCasce, J. H. and Ohlmann, C.: Relative dispersion at the surface of the Gulf of Mexico, *J. Mar. Res.*, 61, 285–312, <https://doi.org/10.1357/002224003322201205>, 2003.
- Lapeyre, G. and Klein, P.: Impact of the small-scale elongated filaments on the oceanic vertical pump, *J. Mar. Res.*, 64, 835–851, <https://doi.org/10.1357/002224006779698369>, 2006.
- 715 Lehahn, Y., d'Ovidio, F., Lévy, M., and Heifetz, E.: Stirring of the northeast Atlantic spring bloom: A Lagrangian analysis based on multi-satellite data, *J. Geophys. Res.*, 112, C08005, <https://doi.org/10.1029/2006JC003927>, 2007.
- Lekien, F., Coulliette, C., Mariano, A. J., Ryan, E. H., Shay, L. K., Haller, G., and Marsden, J.: Pollution release tied to invariant manifolds: A case study for the coast of Florida, *Physica D*, 210, 1–20, <https://doi.org/10.1016/j.physd.2005.06.023>, 2005.
- Lucas, J., Koester, I., Wichels, A., Niggemann, J., Dittmar, T., Callies, U., Wiltshire, K. H., and Gerdts, G.: Short-term
- 720 dynamics of North Sea bacterioplankton-dissolved organic matter coherence on molecular level, *Front. Microbiol.*, 7:321, <https://doi.org/10.3389/fmicb.2016.00321>, 2016.
- Meyerjürgens, J., Ricker, M., Schakau, V., Badewien, T. H., and Stanev, E. V.: Relative dispersion of surface drifters in the North Sea: The effect of tides on mesoscale diffusivity, *JGR Oceans*, 124, e2019JC015925, <https://doi.org/10.1029/2019JC015925>, 2020.
- Molcard, A., Andrew C, P., and Özgökmen, T. M.: Directed drifter launch strategies for Lagrangian data assimilation using hyperbolic
- 725 trajectories, *Ocean Model.*, 12, 268–289, <https://doi.org/10.1016/j.ocemod.2005.06.004>, 2006.
- Olascoaga, M. J., Beron-Vera, F. J., Haller, G., Triñanes, J., Iskandarani, M., Coelho, E. F., Haus, B. K., Huntley, H. S., Jacobs, G., Kirwan Jr., A. D., Lipphardt Jr., B. L., Özgökmen, T. M., Reniers, A. J. H., and Valle-Levinson, A.: Drifter motion in the Gulf of Mexico constrained by altimetric Lagrangian coherent structures, *Geophys. Res. Lett.*, 40, 6171–6175, <https://doi.org/10.1002/2013GL058624>, 2013.
- Orre, S., Gjevik, B., and LaCasce, J. H.: Characterizing chaotic dispersion in a coastal tidal model, *Cont. Shelf Res.*, 26, 1360–1374, <https://doi.org/10.1016/j.csr.2005.11.015>, 2006.
- 730 Peacock, T. and Haller, G.: Lagrangian coherent structures: the hidden skeleton of fluid flows, *Phys. Today*, 66, 41–47, <https://doi.org/10.1063/PT.3.1886>, 2013.
- Peng, J. and Dabiri, J. O.: Transport of inertial particles by Lagrangian coherent structures: application to predator-prey interaction in jellyfish feeding, *J. Fluid Mech.*, 623, 75–84, <https://doi.org/10.1017/S0022112008005089>, 2009.

- 735 Pierrehumbert, R. T. and Yang, H.: Global chaotic mixing on isentropic surfaces, *J. Atmos. Sci.*, 50, 2462–2480, [https://doi.org/10.1175/1520-0469\(1993\)050<2462:GCMOIS>2.0.CO;2](https://doi.org/10.1175/1520-0469(1993)050<2462:GCMOIS>2.0.CO;2), 1993.
- Poje, A. C., Toner, M., Kirwan Jr., A. D., and Jones, C. K. R. T.: Drifter launch strategies based on Lagrangian templates, *J. Phys. Oceanogr.*, 32, 1855–1869, [https://doi.org/10.1175/1520-0485\(2002\)032<1855:DLSBOL>2.0.CO;2](https://doi.org/10.1175/1520-0485(2002)032<1855:DLSBOL>2.0.CO;2), 2002.
- Press, W. H., Teukolsky, S. A., Vetterling, W. T., and Flannery, B. P.: *Numerical Recipes in FORTRAN - The Art of Scientific Computing*,
740 Cambridge University Press, Cambridge, UK, 2 edn., 1992.
- Ricker, M. and Stanev, E. V.: Circulation of the European northwest shelf: a Lagrangian perspective, *Ocean Sci.*, 16, 637–655, <https://doi.org/10.5194/os-16-637-2020>, 2020.
- Sansón, L. Z., Pérez-Brunius, P., and Sheinbaum, J.: Surface relative dispersion in the southwestern Gulf of Mexico, *J. Phys. Oceanogr.*, 47, 387–403, <https://doi.org/10.1175/JPO-D-16-0105.1>, 2017.
- 745 Sapsis, T. and Haller, G.: Inertial particle dynamics in a hurricane, *J. Atmos. Sci.*, 66, 2481–2492, <https://doi.org/10.1175/2009JAS2865.1>, 2009.
- Sapsis, T., Peng, J., and Haller, G.: Instabilities on prey dynamics in jellyfish feeding, *Bull. Math. Biol.*, 73, 1841–1856, <https://doi.org/10.1007/s11538-010-9594-4>, 2011.
- Scales, K. L., Hazen, E. L., Jacox, M. G., Castruccio, F., Maxwell, S. M., Lewison, R. L., and Bograd, S. J.: Fisheries bycatch risk to marine
750 megafauna is intensified in Lagrangian coherent structures, *PNAS*, 115, 7362–7367, <https://doi.org/10.1073/pnas.1801270115>, 2018.
- Schrum, C.: Thermohaline stratification and instabilities at tidal mixing fronts: results of an eddy resolving model for the German Bight, *Cont. Shelf Res.*, 17, 689–716, [https://doi.org/10.1016/S0278-4343\(96\)00051-9](https://doi.org/10.1016/S0278-4343(96)00051-9), 1997.
- Schulz, J.-P. and Schättler, U.: Kurze Beschreibung des Lokal-Modells Europa COSMO-EU (LME) und seiner Datenbanken auf dem
755 Datenserver des DWD, https://www.dwd.de/SharedDocs/downloads/DE/modelldokumentationen/nwv/cosmo_eu/cosmo_eu_dbbeschr_201406.pdf?__blob=publicationFile&v=3, 2014.
- Serra, M. and Haller, G.: Objective Eulerian coherent structures, *Chaos*, 26, 053 110, <https://doi.org/10.1063/1.4951720>, 2016.
- Serra, M., Sathe, P., Rypina, I., Kirincich, A., Ross, S. D., Lermusiaux, P., Allen, A., Peacock, T., and Haller, G.: Search and rescue at sea
aided by hidden flow structures, *Nat Commun*, 11, 2525, <https://doi.org/10.1038/s41467-020-16281-x>, 2020.
- Shadden, S. C., Lekien, F., and Marsden, J. E.: Definition and properties of Lagrangian coherent structures from finite-time Lyapunov
760 exponents in two-dimensional aperiodic flows, *Physica D*, 212, 271–304, <https://doi.org/10.1016/j.physd.2005.10.007>, 2005.
- Shadden, S. C., Lekien, F., Paduan, J. D., Chavez, F. P., and Marsden, J. E.: The correlation between surface drifters and coherent structures
based on high-frequency radar data in Monterey Bay, *Deep-Sea Res. II*, 56, 161–172, <https://doi.org/10.1016/j.dsr2.2008.08.008>, 2009.
- Simpson, J. H. and Pingree, R. D.: Shallow sea fronts produced by tidal stirring, in: *Oceanic Fronts in Coastal Processes*, edited by Bowman, M. J. and Esaias, W. E., pp. 29–42, Springer, Berlin, https://doi.org/10.1007/978-3-642-66987-3_5, 1978.
- 765 Smagorinsky, J.: General circulation experiments with the primitive equations, I. the basic experiment, *Mon. Weather Rev.*, 91, 99–164, [https://doi.org/http://dx.doi.org/10.1175/1520-0493\(1963\)091<0099:GCEWTP>2.3.CO;2](https://doi.org/http://dx.doi.org/10.1175/1520-0493(1963)091<0099:GCEWTP>2.3.CO;2), 1963.
- Smith, S. and Banke, E.: Variation of the sea surface drag coefficient with wind speed, *Q. J. Roy. Meteor. Soc.*, 101, 665–673, <https://doi.org/10.1002/qj.49710142920>, 1975.
- Stanev, E. V., Schulz-Stellenfleth, J., Staneva, J., Grayek, S., Grashorn, S., Behrens, A., Koch, W., and Pein, J.: Ocean forecasting for the
770 German Bight: from regional to coastal scales, *Ocean Sci.*, 12, 1105–1136, <https://doi.org/10.5194/os-12-1105-2016>, 2016.

- Stanev, E. V., Badewien, T. H., Freund, H., Grayek, S., Hahner, F., Meyerjürgens, J., Ricker, M., Schöneich-Argent, R. I., Wolff, J.-O., and Zielinski, O.: Extreme westward surface drift in the North Sea: Public reports of stranded drifters and Lagrangian tracking, *Cont. Shelf Res.*, 177, 24–32, <https://doi.org/10.1016/j.csr.2019.03.003>, 2019.
- 775 Sudharsan, M., Brunton, S. L., and Riley, J. J.: Lagrangian coherent structures and inertial particle dynamics, *Phys. Rev. E*, 93, 033 108, <https://doi.org/10.1103/PhysRevE.93.033108>, 2016.
- Sündermann, J. and Pohlmann, T.: A brief analysis of the North Sea physics, *Oceanologia*, 53, 663–689, <https://doi.org/10.5697/oc.53-3.663>, 2011.
- Sutherland, G., Soontiens, N., Davidson, F., Smith, G. C., Bernier, N., Blanken, H., Schillinger, D., Marcotte, G., Röhrs, J., Dagestad, K.-F., Christensen, K. H., and Breivik, Ø.: Evaluating the leeway coefficient for different ocean drifters using operational models, *arXiv:2005.09527 [physics.ao-ph]*, 2020.
- 780 Teeling, H., Fuchs, B. M., Becher, D., Klockow, C., Gardebrecht, A., Bennke, C. M., Kassabgy, M., Huang, S., Mann, A. J., Waldmann, J., Weber, M., Klindworth, A., Otto, A., Lange, J., Bernhardt, J., Reinsch, C., Hecker, M., Peplies, J., Bockelmann, F. D., Callies, U., Gerdt, G., Wichels, A., Wiltshire, K. H., Glöckner, F. O., Schweder, T., and Amann, R.: Substrate-controlled succession of marine bacterioplankton populations induced by a phytoplankton bloom, *Science*, 336(6081), 608–611, <https://doi.org/10.1126/science.1218344>, 2012.
- 785 Thiel, M., Hinojosa, I. A., Joschko, T., and Gutow, L.: Spatio-temporal distribution of floating objects in the German Bight (North Sea), *J. Sea Res.*, 65, 368–379, <https://doi.org/10.1016/j.seares.2011.03.002>, 2011.
- Tian, F., He, Q., Liu, Z., and Chen, G.: Extracting Lagrangian coherent structures in the Kuroshio current system, *Ocean Dyn.*, 69, 641–656, <https://doi.org/10.1007/s10236-019-01262-6>, 2019.
- 790 van Sebille, E., Griffies, S. M., Abernathey, R., Adams, T. P., Berloff, P., Biastoch, A., Blanke, B., Chassignet, E. P., Cheng, Y., Cotter, C. J., Deleersnijder, E., Döös, K., Drake, H. F., Drijfhout, S., Gary, S. F., Heemink, A. W., Kjellsson, J., Koszalka, I. M., Lange, M., Lique, C., MacGilchrist, G. A., Marsh, R., Mayorga Adame, C. G., McAdam, R., Nencioli, F., Paris, C. B., Piggott, M. D., Polton, J. A., Rühls, S., Shah, S. H., Thomas, M. D., Wang, J., Wolfram, P. J., Zanna, L., and Zika, J. D.: Lagrangian ocean analysis: Fundamentals and practices, *Ocean Modelling*, 121, 49 – 75, <https://doi.org/10.1016/j.ocemod.2017.11.008>, 2018.
- 795 Wiggins, S.: The dynamical systems approach to Lagrangian transport in oceanic flows, *Annu. Rev. Fluid Mech.*, 37, 295–328, <https://doi.org/10.1146/annurev.fluid.37.061903.175815>, 2005.